Performance of a hydrogen fuel cell scooter used for combined transport and residential power production





Performance of a hydrogen fuel cell scooter used for combined transport and residential power production

L.B. van Leeuwen

To obtain the degree of

Master of Science

in Sustainable Energy Technology

at the Delft University of Technology,

To be defended publicly on Thursday November 22, 2018 at 9:30.

Student number: 4524136

Supervising professor: Prof. dr. A. van Wijk TU Delft
Daily supervisor: Dr. C. Robledo TU Delft
Thesis committee: Prof. dr. ir. Z. Lukszo TU Delft
Dr. A. Purushothaman Vellayani TU Delft

An electronic version of this thesis is available at http://repository.tudelft.nl/.



Preface

You are about to read the dissertation "Performance of a hydrogen fuel cell scooter used for combined transport and residential power production". It has been written to fulfill the graduation requirements of the Master of Science Sustainable Energy Technology at Delft University of Technology. This thesis is also part of my second Master of Science Biotechnology which I follow at Wageningen University. I have been working on this project from March to November 2018.

The project was initiated by Professor Ad van Wijk, which is a fervent believer in the green hydrogen economy. The research question was formulated together with my daily supervisor Dr. Carla Robledo. This project combined practical lab-work with data analysis while covering diverse fields of research, ranging from electrochemistry to mechanical engineering. The results from this thesis were presented in Japan at the International Symposium on Hydrogen Energy and Energy Technologies (HEET) and have been accepted for publication in a special edition of the International Journal of Hydrogen Energy.

In the coming paragraph, I would like to express my gratitude to all the people who have helped me throughout this project.

I would like to express my appreciation to Ad for facilitating this thesis and welcoming me into the Future Energy Systems group. Thank you for the helpful CaPP meetings.

I would especially like to thank Carla for her guidance throughout the project. This journey was diverse, from opening up the scooter with screw drivers to writing a paper manuscript together. I really appreciated this collaboration and learned a lot from you. I am very thankful for your critical feedback as well as your patience and understanding. You were the backbone of my work, thank you!

Thank you to Lars Kiewidt for keeping an eye on me from Wageningen. Also, I am grateful to the lab technicians Jaap and Martijn which helped me with my project whenever I needed. I am not a specially talented scooter mechanic, so your help was really appreciated.

Now I would like to thank the outsiders of my thesis, which did not help for the content but without whom I would not have completed this work. My time gradating was intrinsically linked with my current medical condition. Sometimes this made the journey feel like I was driving on the TMDC: in between the bursts of acceleration, I had moments of deceleration and even stand still. Luckily, Dr. K and his amazing team kept me in shape throughout the entire process. They deserve a particular note of thanks for both their medical support and their strong belief in me reaching my (academic) goals.

Last but not least, I am grateful to my family and friends which supported me throughout the

iv Preface

project. Counselling, wise words of support and reviewing my writing: you helped a lot making this thesis.

I hope you enjoy your reading.

L.B. van Leeuwen Delft, November 2018

Abstract

A hydrogen fuel cell scooter was tested for the first time to alternatively drive, power electric appliances (Vehicle-to-Load, V2L) and power the grid (Vehicle-to-Grid, V2G). Performance of the scooter is known to rely mainly on the fuel cell stack, and fuel cell degradation depends on the operating conditions. This study aimed to provide insights on how each mode of operation (driving, V2L and V2G) impacts the fuel cell stack performance, as well as the overall system. Operation in each mode was mimicked by applying typical duty cycles to the hydrogen scooter via an electronic programmable load. Analysis of the experimental data yielded clear differences between each mode of operation. Principal Component Analysis (PCA) revealed that the voltage of the fuel cell and the battery were most determining in segregating the three modes. The highest system efficiency was found for V2G usage of the scooter (39.4% based on higher heating value). The power demand throughout this mode was high, making the fuel cell operate at almost full capacity. Linear regression analysis was used to determine the fuel cell degradation rate. Severe degradation was measured throughout the experiments, with an overall voltage cell drop of 402 μV/h. Distinguishing the degradation rate per mode revealed V2L operation to cause the largest fuel cell degradation (648 μ V/h) and driving the least degradation (205 μ V/h). This result was confirmed by comparing the IV curve of the fuel cell stack before and after the experiments: the largest voltage drop occurred at low currents. Further research on scooter usage in combined modes should include new energy management strategies for V2G and V2L operation, which focus on minimizing fuel cell degradation.

Contents

Li	st of	Figures	ix
Li	st of	Tables	хi
1	Intr	roduction	1
	1.1	Problem statement	1
	1.2	A complete energy transition	2
		1.2.1 The energy and the transport transition	2
		1.2.2 Integration of fuel cell vehicles in the power production system	3
	1.3	Status of fuel cell voltage durability studies	6
	1.4	Research question	7
2	Mat	erials and methods	9
	2.1	Research design	9
	2.2	Characterization of the fuel cell scooter	10
		2.2.1 Fuel cell system	11
		2.2.2 Battery components	15
		2.2.3 System configuration and control	16
		2.2.4 Balance of Plant	16
	2.3	Design of the duty cycles	18
		2.3.1 Driving mode	18
		2.3.2 Vehicle-to-Load mode	19
		2.3.3 Vehicle-to-Grid mode	20
		2.3.4 Comparison of the duty cycles	20
	2.4	Experimental procedure	20
	2.5	Data analysis	22
3	Res	ults	25
	3.1	Operation of the power system in the different mode	25
		3.1.1 Power dynamics	25
		3.1.2 Distribution of variables per mode	27

viii Contents

	3.2	Balance of plant components	. 29
	3.3	System efficiency	. 31
	3.4	Ordination of the modes according to the variables	. 33
	3.5	Fuel cell degradation rates	. 35
		3.5.1 Overall voltage decline rate	. 35
		3.5.2 Mode-wise degradation rate	. 37
	3.6	Voltage drop as a function of current	. 39
4	Inte	erpretation of the results	43
	4.1	The scooter in the energy system	. 43
	4.2	Scooter used for driving	. 44
	4.3	Scooter used in V2G mode	. 45
	4.4	Scooter used in V2L mode	. 47
	4.5	Degradation of the fuel cell stack	. 48
5	Disc	cussion	51
	5.1	Remarks on the setup and assumptions	. 51
		Recommendations for future work	
6	Con	clusion	53
ъ.			
ы	DIIOG	raphy	55
A	TMI	OC: from velocity to instantaneous power demand	59
	A.1	Model structure	. 59
	A.2	Model parameters	. 60
В	List	of experiments	63
C	Cali	bration curves	65
	C.1	Pressure calibration	. 65
	C.2	Current calibration	. 65
	C.3	Hydrogen mass calibration	. 66
		C.3.1 Linear fit from voltage signal	. 66
		C.3.2 Corrected Faraday consumption	. 67
		C.3.3 Measured masses with idling time correction	. 67
		C.3.4 Summary	. 68
D	Ene	rgy management strategy in V2L experiments	71

List of Figures

1.1	Generalized polarization curve for fuel cells	7
2.1	Pictures of the APFCT hydrogen fuel cell scooter. a) Front view of the scooter. b) Hy-	
	drogen storage canisters being clicked in the rear part of the scooter	10
2.2	Schematic hydrogen fuel cell with electrode reactions	12
2.3	Working principle of a metal hydride: the cube of grey atoms represents the metal	
	lattice. Each red dot is a hydrogen atom, which can be inserted into the voids of the	
	metal structure. This process releases heat.	14
2.4	Metal hydride canister and its holder	14
2.5	Fueling set-up in the lab	15
2.6	Electrical diagram of the main power components in the scooter and location of the	
	current sensors installed	16
2.7	Architecture of the supply systems and BoP	17
2.8	Steps in TMDC modification	19
2.9	Power consumption signal of 3 household appliances sampled for 900s of operation	20
2.10	Final V2L duty cycle designed to match the characteristics of the electronic load	20
2.11	Duty cycle designed per mode	21
2.12	Load duration curve for each mode	22
2.13	Connection cable between the scooter and the electronic load	23
2.14	Schematic view of the course of an experiment	23
3.1	Energy management for a typical duty cycle, per type of experiment	26
3.2	Data distributions under the V2G, drive and V2L modes, corresponding to the variables	
	a) FC voltage, b) battery voltage and c) output voltage, d) FC current, e) battery current,	
	f) output current, g) temperature of the FC, h) pressure within the canisters, i) mass	
	of hydrogen present in the canisters. Central points within the boxplots represent the	
	average value; boxes mark the 25th and 75th percentiles and the segment within the	
	box represents the median; segments outside the box mark the values that extend 1.5	
	times the width of the box; points outside are outliers	28
3.3	Effect of the fan on BoP power consumption and temperature of the FC in a V2G experiment $$	30
3.4	Power delivered by FC as a function of temperature	30
3.5	IV curve battery	32

x List of Figures

3.6	PCA results	34
3.7	Variance of the data explained per principal components	35
3.8	Regression model fit for voltage as a function of accumulated time	37
3.9	Regression model fit for voltage as a function of accumulated time per mode	39
3.10	Polarization curves of the scooter's FC stack	40
3.11	Regression lines per mode for voltage fuel cell as a function of current	41
4.1	Energy system of the hydrogen fuel cell scooter: from renewable electricity generation to multi-modal scooter usage	44
A.1	Free-body diagram of the scooter	59
A.2	TMDC in power units, as converted by the physical model	61
B.1	Order and time of experiments	64
C.1	Calibration curve of the hydrogen mass contained in the canisters	67
C.2	Real mass of hydrogen against estimates from Faraday's law	68
D.1	Allocation of power sharing between the fuel cell and the battery for each of the V2L	
	experiments, in the order they were performed	72
D 2	SOC of the battery throughout the whole experimental period	73

List of Tables

2.1	Specifications of the fuel cell, battery and canister in the scooter	11
2.2	Characteristics of the original and modified TMDC	19
3.1	Average value for the consumed hydrogen and system efficiency per mode	32
3.2	Distribution and descriptive statistics of the hydrogen consumption values [g H2]	33
3.3	Eigenvectors of each variables per PC	35
3.4	Regression coefficients for fuel cell voltage modelled as a function of cumulative time	
	without distinction of mode	36
3.5	Regression coefficients for fuel cell voltage modelled as a function of cumulative time	
	per mode	38
3.6	Degradation rate and estimated lifetime of an average fuel cell in the fuel cell stack of	
	the scooter for each mode	39
3.7	Regression coefficients of the IV relationships per mode	41
A.1	Model parameters for TMDC	61
C.1	Average hydrogen consumption per mode in gram	69
D.1	V2L experiments per EM category	73

1

Introduction

Scooters have been defining our landscapes since the 1950's. As the second world war had ravaged the European economy, a cheaper alternative to the automobile was sought for. This materialized as the scooter. The iconic Vespa was created in Italy by Enrico Piaggo, as his aircraft factory was loosing momentum towards the end of the war. A new era of affordable individual mobility had started. First spreading throughout Europe, the scooter quickly took over the other continents. Each country ended up developing its own motorized two-wheeler, Japan and the US joining Italy in leading the market with the introduction of the Harley-Davidson and the Fuji Rabbit [1].

As of today, scooters remain a popular means of transportation. In an increasingly urbanized world, they offer flexibility for daily commuting and are easy to park. Most of all, scooters remain the affordable alternative to personal cars and are especially popular in countries knowing economic development. Up to 95% of the motor vehicles on road in Asia are motorcycles [2], as convenient affordable urban transport is especially needed there. Scooters are also easy to maneuver through dense traffic, which is a key advantage in densely populated areas.

1.1. Problem statement

Motorization of individuals in cities is leading to severe consequences, predominantly on local air quality. Besides carbonated emissions, volatile compounds and particulate matter represent threats to both the environment and public health. Recent research has reported two-stroke scooters to be a dominant cause of urban vehicular pollution, above cars and trucks [3]. Mitigation measures are needed to safeguard both future generations and their living environment.

1. Introduction

The threat on environmental and public health have led governments to commit themselves to reduce the emission of greenhouse gases (GHG). In Paris 2015, 195 governments agreed on limiting emissions such that the global average temperature does not exceed a 2° C increase since pre-industrial times [4]. To reach this, profound changes must be made in the current systems driving our society's economy. Comparing the emissions by sectors, it appears that 25% of the anthropogenic GHG emissions come from electricity and heat production, and 14% from the transport sector. Both sectors represent the pillars of development and are needed to provide people with a good quality of life. A mitigation strategy is needed which lowers emissions from the energy and the transport sectors without reducing people's quality of life [5].

1.2. A complete energy transition

1.2.1. The energy and the transport transition

Future requirements for the energy and transport sectors include sustainability, reliability and affordability while safeguarding the comfort of the end-user. To reach these goals, profound changes need to be made.

First of all, renewable energy sources (RES) are thought to provide sustainable, emission-free power supply. However, a transition from fossil to renewable energy use carries many challenges. Renewable energy sources, such as wind and solar are dependent on weather conditions. The power generation is intermittent, and cannot be controlled in the same way as the traditional coal or gas-fired power plant. A more flexible power system will be required to ensure reliability of supply and secure the grid, to prevent curtailment. Systems such as storage or smart grids can provide solutions for this [6]. A smart grid is a local unit where energy is produced, transformed and consumed. Flexibility is created by physical storage instruments as well as market instruments, such as electrical storage units, conversion to fuel, controllers or price indexing. These components must balance the micro-level generation and consumption together with the macro-level interconnections [7].

Second, future transport systems will move from combustion engines to electrically-driven engines. Electric motors have numerous advantages: they are more efficient, have fewer moving parts (only a rotor) which allows for a lighter, more compact and inexpensive engine, and they can run on RES without having emissions affecting health and climate. In the past, the implementation of electrical motors has been hindered by low energy density of batteries and the high cost of electrochemical storage systems. This is changing rapidly, making electric vehicles (EVs) cost-competitive in the coming years. There are two forms of EVs, the Battery Electric Vehicle (BEV) and the Fuel Cell Electric Vehicle (FCEV). While the BEV gets its electricity to drive the motor from electricity storage in a battery, the

FCEV gets it from a fuel, for example hydrogen, which is transformed on-board to electricity in a fuel cell. Advantages of hydrogen FCEVs are the extended driving range and the fast refueling. Moreover, hydrogen might be a key player to increase grid flexibility, as more loads will be electric in the future while energy sources are intermittent. Hydrogen can act as a buffer to avoid curtailment. In general, a transition to electric driving is seen as necessary [8]. Governments such as Taiwan have been encouraging zero-emission two-wheelers by regulating gasoline engines and subsidizing electric scooters instead [9].

When rethinking the energy and transport infrastructure, new energy carriers might come into play. Hydrogen has the potential of becoming a key player in these transitions as it possesses the major advantage of producing only water as by-product when used in fuel cells for electricity production. Hydrogen is an energy carrier, not a source of energy. This means it must be produced by an energy source which is sustainable in order to meet the goals mentioned here-above. Production from water electrolysis using renewable electricity is a way to produce this sustainable, so-called "green hydrogen". With large scale solar and wind energy becoming cheaper sources of electricity, new sustainable methods to transport this affordable electricity are needed. Hydrogen can fulfill this role. Hydrogen can be produced on-site at the wind or solar farm. Then it can be compressed, liquified or turned to ammonia using nitrogen from the air to make it convenient to transport. Finally, hydrogen can be shipped or piped to the end-user for consumption. In this way, hydrogen can act as a buffer for renewable electricity storage and distribution [10]. Using hydrogen is however mostly relevant for inter-seasonal purposes and long distance transport of energy. Batteries might be a more effective solution to provide short-term intra-day energy storage [11].

The energy transition and the transport system transition translate into the creation of new infrastructure. This implies huge capital and operational costs. However, experts believe integrating the transportation and electric infrastructure would decrease the economic burden caused by such transitions. This statement is based on the fact that personal vehicles are used only 5% of the time for transportation purposes. As a result, they are available 95% of the time for other types of usage, for example absorbing or producing power [12]. Such a symbiotic integration of the energy and transport systems is thought to reduce the cost-barrier in the transition of both sectors towards a more sustainable future [13].

1.2.2. Integration of fuel cell vehicles in the power production system

The idea of integrating cars in the electric grid emerged in the 1990's. Kempton and Letendre, from the university of Delaware, initiated scientific interest in using EVs not only as a load but also as a source of power [14]. Since then, studies have been conducted on many aspects of this promising technology.

4 1. Introduction

It appears that the applications of this concept are numerous, and the potential is real.

Electric cars have the potential of absorbing or delivering up to 10 kW to the grid when in idling state [14]. Europe's electrical fleet reached one million EVs in 2018, which translates into a potential capacity of 10 GW electricity supply [15]. This means the current electric fleet represents already 1% of the European installed electric capacity (989 GW electricity, [16]). Assuming EVs become pervasive in the future and take over totally the passenger fleet, passengers vehicles could represent 2.5 times the installed electricity capacity of Europe (252 million vehicles for 989 GW installed capacity [17]).

The Green Village is a living lab initiative at Delft University of Technology. Testing of innovations before implementation on pilot scale is facilitated. One of the projects being run at the Green Village is the Car as a Power Plant (CaPP), in which a hydrogen FCEV is used for combined transportation and electricity production [12]. The research going on is focusing on FCEV only as these vehicles proved their superiority over BEVs in terms of refuelling (3 min on average) and driving radius (500 km). Experts believe penetration of FCEVs to increase in the future as they have been demonstrated to represent a technologically and economically viable alternative to incumbent vehicles [18]. FCEVs are commercially available, with models such as the Hyundai ix35 [19], the Toyota Mirai [20] or the Honda Clarity [21]. The spreading of fuel cell electric scooters (FCES) is also being geared up, with demonstration projects going on in Taiwan on scooters from APFCT and in the UK as the Londoner Met Police is driving on Suzuki's Burgman scooter [22–24]. Though FCEVs are in the first steps of market penetration, hydrogen as an energy carrier for vehicles is gaining momentum internationally. Both the Japanese and the German government are investing in hydrogen fuelling infrastructure to meet up the fleet development [25, 26].

In literature, the union of electric vehicles and the electricity grid is called Vehicle-to-Grid (V2G). In this concept, the assumption is made that EVs will be widely adopted in the future and can thus be integrated in stationary energy system to receive and supply energy. V2G applications exist on different scales, from the national scale to a single dwelling. These applications are outlined hereafter.

A vehicle used in V2G can either receive or deliver electricity to the national grid. As a result, the car acts as a mobile energy storage unit which balances the electricity grid to ensure its stability. In future energy systems, grid stability will not be provided by centralized power plants anymore, as there are running mainly on fossil fuels. New frequency reserves from sustainable sources are sought for, and the Car Park as Power Plant (CPPP) offers such possibility. In her research, Michelle Poorte analyzed the impact of a car park containing FCEVs on the electricity network and demonstrated its technical suitability to offer fast frequency reserves [27]. This V2G application is of large scale type, aiming to stabilize the grid on national level. As national grids are connected to nearby countries, V2G application is possible on international level. However, this means the car is not taken as an entity anymore but

the car park is.

Other applications of EVs in providing electricity take place at the smart grid scale. In a demonstration project at the Green Village, Robledo *et al.* showed how a hydrogen FCEV can act as a local power source. The system included an all-electric house, with solar panels for electricity production. The vehicle was used for both mobility and power production purposes, and helped the local unit to reduce its annual electricity import from the national utility grid by 71% [28].

The concept of using a vehicle as a source of power reaches beyond its use for grids. In fact, any power sink could be connected to a vehicle, so-called vehicle-to-X applications (V2X). V2X is a collective term which includes the three following categories:

- Vehicle-to-Load (V2L), in which a vehicle provides power supply to electric appliances directly
- Vehicle-to-Home (V2H), where the vehicle is used to power homes in times of electric shortage
- Vehicle-to-Grid (V2G), in which a group of vehicles is used to stabilize the grid, or single vehicles are used for smart-grids.

In V2L and V2H applications, there is no coordination with the grid system operator: control and operation of the EV is local and independent of the larger electricity grid. This increases the degrees of freedom related to its usage. V2L and V2H can for example be used on remote sites such as military hospitals or construction sites, where no connection to the grid is available.

Vehicle-to-Load technology is especially interesting in the case of using a scooter as a power provider. The scooter's capacity is rated at 1 kW on average, which is only 10% of the power capacity of a FCEV passenger car. As a consequence, the applications of the use of a scooter in V2X are very different than the car's. V2L seems a more appropriate application than V2G for example: the relative effect of the scooter on a national grid seems negligible. However, scooters could be used for loads which require less than 1 kW power. A typical example would be to use the electric scooter as power source during a camping holiday in a remote area, to power an electric stove or charge a phone.

Integration of EVs with the electrical infrastructure appears to have very diverse applications, ranging from large to small scale depending on the type of vehicle. Such a synthesis benefits in two ways. On the one hand, it fosters the penetration of EVs on the market which leads to environmental and health benefits. On the second hand, it stimulates the transition from centralized fossil energy supply to more efficient and versatile decentralized sustainable energy system.

6 1. Introduction

1.3. Status of fuel cell voltage durability studies

Performance of vehicles is very much dependent on its usage. Different driving cycles can cause more or less degradation of the different vehicle components. The main component of a FCEV is the electric motor, which replaces the traditional combustion motor. Energy for the motor is provided by a main power source, the fuel cell which is fed with hydrogen. A peaking power battery is used as a back-up power source to provide power beyond the FC operation range. This design is advantageous, allowing for a smaller sizing of the FC and thus cost and volume reduction. Among these components, the main bottleneck remains the fuel cell system (FCS). Therefore, understanding of the main degradation processes endured by the FCS is necessary [29]. Degradation stands for a performance reduction in time and is usually measured as a voltage loss in μV per hour of usage. Losses in fuel cells are the reflection of the hydrogen's Gibbs free energy not being converted into electrical energy. Previous research has identified different types of losses, which are summarized here [11].

Activation losses are caused by the slowness of the reactions taking place at the surface of the electrodes. Part of the voltage generated is used to transfer the electrons towards and from the electrodes. This voltage drop is non-linear.

Ohmic losses are the resistance to the flow of electrons through the electrodes, the interconnects and the electrolyte, and is proportional to the current density and thus linear.

Mass transport losses result from the change in concentration of the reactants at the surface of the electrodes because the fuel is being consumed. The concentration is the reactant decreases and there is not sufficient mass transport to the electrode surface to compensate the loss. From the Nernst equation, it is known that a change in concentration will directly affect the voltage.

Fuel crossover and internal currents are the losses linked to the electrolyte: fuel or electrons are crossing through.

Each of these losses causes a decrease of the voltage compared to the ideal voltage. Depending on the current (density) at which these losses occur, one can identify the type of loss mainly responsible for the reduction in performance. In figure 1.1, the main losses and their dominant regions are described. Such a curve is called an IV or polarization curve and depicts the DC voltage delivered at the terminals of the cell against the current density drawn by an external load. Polarization is a synonym for loss or irreversibility.

Closely controlled studies as well as theoretical models have been proposed to explain the losses in fuel cell used on-board of vehicles. However, only a few studies have been found on more real-life testing of fuel cell vehicles. These studies provide important information on the complex working of hybrid fuel cell vehicles.

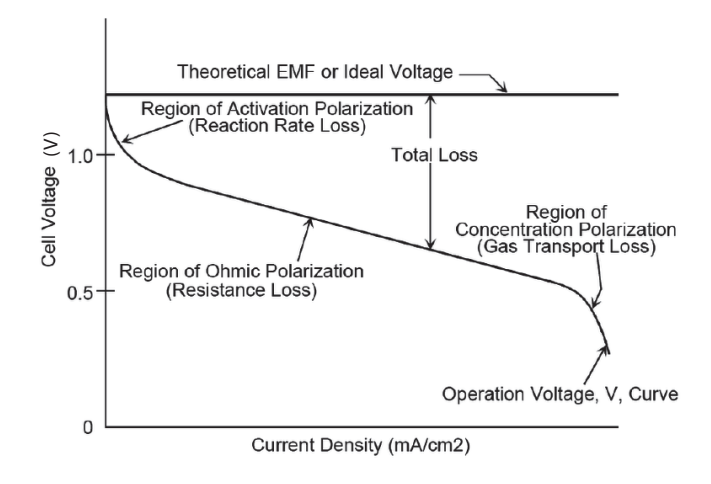


Figure 1.1: Generalized polarization curve for fuel cells

Li *et al.* performed on-road testing of a plug-in hybrid fuel cell city bus. For one year, the fuel cell city bus was operated on a fixed city route in Beijing. The power demand of the fuel cell city bus was nearly stable. This resulted in an average FC decline rate of 346 μ V/h at a current density of 120 A, which is considered to be a large degradation rate. A close look was taken into voltage uniformity throughout the tests, as voltage uniformity worsens along with degradation. Increasing ohmic losses were the main cause of voltage drop and decline in voltage uniformity [29]. In another study setup by the American NREL, real world operating data of 90 fuel cell vehicles from different brands was gathered [30]. This study covers a broad variety of topics, from fuel cell durability to filling behavior of the drivers. Between 2006 and 2015, the average fleet fuel cell stack's durability increased from about 1000 operating hours to 2,200 operating hours. Improved voltage durability has led to increasing lifetime of the FC stacks and thus vehicles.

Considering the need for more integrated power and transport system, it is important to understand the consequences of multi-purpose usage of a fuel cell electric vehicle on its performance. While Li et al. and Jennifer et al. focused on vehicles driving only, Oldenbroek et al. compared vehicle fuel cell stack voltage degradation in driving and V2G modes. Four commercial Hyundai ix35 FCEVs were used for driving, idling and V2G operation. No clear correlation was found between voltage drop and time of operation, energy produced or driven distance. From there, it was suggested to analyze a more extensive combination of parameters to predict fuel cell decay in vehicles used for multiple purposes [31].

1.4. Research question

All in all, the influence of the different V2X modes on FC degradation in FCEV remains a relatively uncovered topic in literature. Only a bus and the passenger car were covered until now. In this study,

8 1. Introduction

a hydrogen fuel cell electric scooter (FCES) is used to test its fuel cell degradation under realistic usage conditions, while being used in three different modes: driving, V2L and V2G. This leads us to formulating the main research question:

How does the combined use of a hydrogen fuel cell scooter for driving, V2L and V2G purposes affect its performance?

To answer the main research question, three sub-questions have been defined, which will be answered throughout this study.

- 1. How does the scooter perform in the three different modes?
- 2. How does the fuel cell degrade in the three different modes?
- 3. Which mode leads to more degradation of the fuel cell?

In the second chapter, the materials and methods used to answer these questions are outlined. Background information on the hydrogen fuel cell scooter is given, typical duty cycles are designed and both the experimental and analysis procedures are presented. The third chapter covers the results from the experiments. The behavior throughout the modes of key system components is explained, such as the fuel cell and the battery dynamics. The efficiency of the system is calculated per mode, and the decay rate of the fuel cell is presented. These results are interpreted in a fourth chapter, where the relevance of these findings to the scientific community is explained. Finally, a discussion and conclusion can be found in the fifth and sixth chapter, which elaborate on the main research question.

Materials and methods

In this chapter, the tools and methodology used to answer the main research question are outlined. The research conducted is quantitative; experiments were performed on a scooter in the TU Delft labs in order to determine the effect of using the vehicle for driving, V2L and V2G on its fuel cell. This chapter is organized as follows. First, the research design is defined. Then, the scooter used in this study is characterized as all its components are described. The design of the duty cycle representing each of the three mode is explained in a third section, followed by a procedure of the experiments. Finally, the methods used in analyzing the gathered data are justified.

2.1. Research design

In chapter 1, the main research question was defined as follows: **how does the combined use of a hydrogen fuel cell scooter for driving, V2L and V2G purposes affect its performance?**. In this study, we aim to study the use of the scooter as close as possible to real-life usage. Therefore, experiments are performed on a real prototype, model 4.8 from APFCT.

The use of the scooter in the different modes was simulated by applying typical duty cycles of each mode on the FCES using a programmable electronic load. An electronic load uses semiconductors as a load instead of the usual resistors, which allows free voltage and current (and thus power) control [32]. The choices made in the design of the duty cycle are justified in section 2.3. It has been chosen to apply the duty cycle of each mode 30 times to the scooter for a duration of 1024 seconds. The number of experiments conducted per mode was chosen as large as possible, while fitting the available time for this study. This study of 30 ECTS represents six months of full-time work. It was chosen to have

one third dedicated to experiments, which leaves 2 months to perform the tests. 90 tests to perform in total in two months resulted in a reasonable amount of 11 tests to perform per week. The total time of the scooter actually delivering power was 25.6 hours.

In order to quantify the effect of the different modes on the fuel cell, different measurements were performed. The variables measured were the following:

- voltage of the FC, battery and output voltage
- current of the FC, battery and output current
- mass of H₂ contained in the canisters
- pressure of H₂ in the canisters
- temperature of the FC and of the canister
- cumulative time since the start of the experiments.

Besides, a polarization curve was made before the start and after completing the experiments. Comparing the initial and final IV curves gives information about the irreversible losses undergone by the fuel cell depending on its operation mode.

2.2. Characterization of the fuel cell scooter

The fuel cell electric scooter used in this study is a model ZES 4.8 from manufacturer APFCT and is illustrated in figure 2.1.



Figure 2.1: Pictures of the APFCT hydrogen fuel cell scooter. a) Front view of the scooter. b) Hydrogen storage canisters being clicked in the rear part of the scooter

The scooter is mainly powered by a low temperature Proton Exchange Membrane type of fuel cell, with rated power 1200 W. The fuel cell is fed with hydrogen, which is stored as a metal hydride in

canisters. These canisters can be clicked in the rear of the scooter, as shown in figure 2.1b. A Liion Nickel-Cobalt-Manganese (NCM) battery is used as a secondary power source, which is placed in parallel in the circuit allowing any combination for power supply (FC or battery only, or FC and battery combined). The rated capacity of the battery pack is 20 Ah. The scooter can only be charged by the hydrogen canisters, there is no electrical plug-in to charge the battery externally. The battery is being charged from the fuel cell. A summary of the FCS and battery specifications can be found in figure 2.1. The Balance of Plant (BoP) are the components which facilitate the operation of the power components. These include an air blower, which feeds in the oxygen, a water pump and a fan, which takes care of cooling. In this section, the working mechanism of the fuel cell scooter is explained further.

Component	Property	Value
PEM Fuel Cell	Rated power	1200 W
	Rated voltage	24 V
	Operating voltage	21-33 V
Li-NMC Battery	Rated capacity	20 Ah
	Material of the metal hydride	AB5 Alloy
Hydrogen Canister	Mass hydrogen stored per canister	45 g

Table 2.1: Specifications of the fuel cell, battery and canister in the scooter

2.2.1. Fuel cell system

Power supply within the scooter is mostly carried out by the fuel cell, which converts chemical energy in the form of hydrogen bonds to electrical energy. The components related to the fuel cell system are: the fuel cell stack, the hydrogen canisters and the blowers.

Fuel cell stack

A fuel cell is an electrochemical engine that produces electricity from paired oxidation/reduction reactions. In a hydrogen fuel cell, the following subreactions take place:

$$2H_2 \to 4H^+ + 4e^-$$
 (2.1a)

$$4e^- + O_2 \rightarrow 2O^{2-}$$
 (2.1b)

This yields the overall reaction described in 2.2.

$$2H_2 + O_2 \rightarrow 2H_2O$$
 (2.2)

In fuel cells, electricity is produced directly from the chemical reaction shown in equation 2.2. As a comparison, combustion engines first produce heat which is then transformed into electricity via a heat engine. The efficiency of this process is dictated by the Carnot limit of operating temperatures.

Physically separating the reaction 2.2 in different parts of the cell differentiates the fuel cell from the combustion engine. The electrodes (anode and cathode) are attached at either sides of the electrolyte. At the anode part of the cell, hydrogen is fed in and split into hydrogen ions and electrons. The electrons flow through an external circuit to provide the desired current while the H⁺ ions are driven through the electrolyte. Electrostatic balance is reached when the hydrogen ions reach the cathode to recombine with oxygen and the electrons to produce water. This process is illustrated in figure 2.2 [11, 33]. In theory, other reducer/oxydizer couples can be used in a fuel cell. Hydrogen has suitably fast reaction kinetics and oxygen is easily retrievable from the air, which justifies their respective usage in this setup. A noble metal catalyst coated on the electrodes reduces the activation energy of the hydrogen and oxygen ionization/recombination process, which accelerates the process of reestablishing an equilibrium as the ions are consumed by the fuel cell. Platinum is used as a catalyst here.

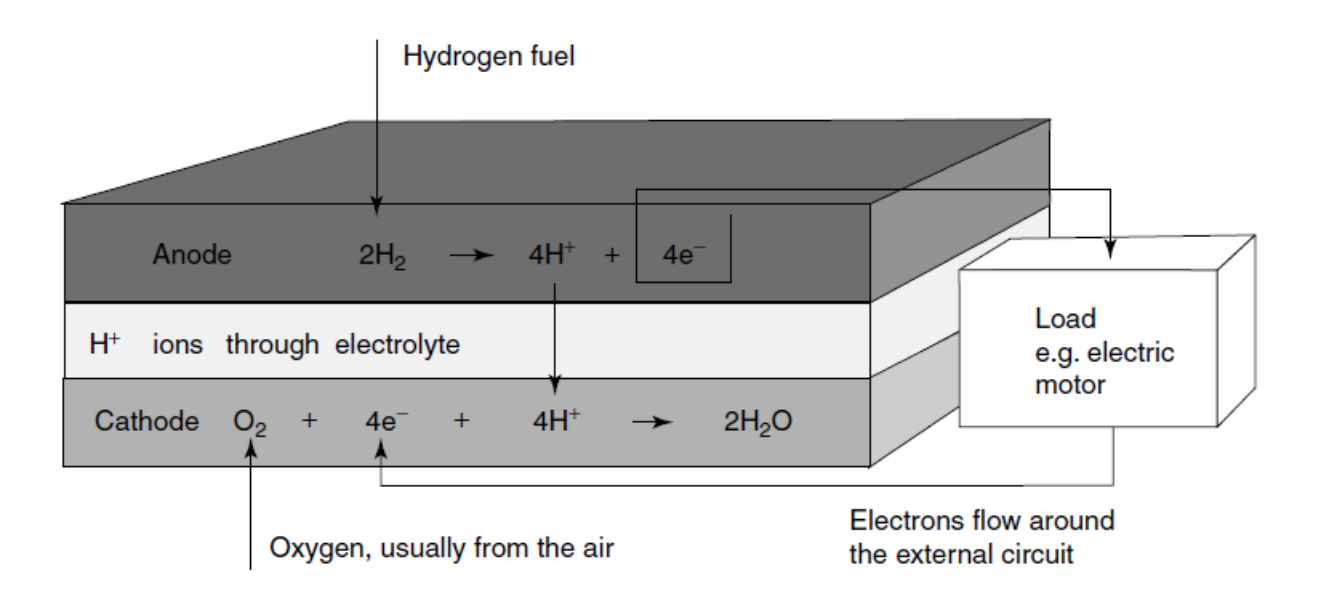


Figure 2.2: Schematic hydrogen fuel cell with electrode reactions

Many different types of fuel cells exist, each type being characterized by different electrolytes and operating temperatures. The "Proton Exchange Membrane" or "Polymer Electrolyte Membrane" fuel cell (PEM or PEMFC) has been receiving most attention for mobile applications and is thus used here. Their operating temperature is relatively low (30-100°C), which gives the advantage of a quick start-up. Also, lower temperatures lead to less wear on the system components and thus a better durability of the fuel cell system. In a PEMFC, the electrolyte is a solid polymer in which the hydrogen protons are mobile. The membranes can be extremely thin, which allows for dense packing and thus high power density [11].

Individual fuel cells are electrically connected in series to create the voltage determined by the

motor. Connected cells form a fuel cell stack. As the nominal voltage delivered by the fuel cell stack of the scooter is known to be 24 V while the stack is formed by 40 cells, an individual fuel cell voltage of 0.6 V can be back-calculated. The same current flows through the entire stack, which is determined by the membrane properties and the individual cell area. In the stack, fuel cells are arranged such that the protons can pass through the membrane while the electrons are conducted through the external circuit. Oxygen and hydrogen is fed to the membranes where they react. Each fuel cell in the stack consists of a MEA, or membrane Electrode Assembly which is a membrane with flat electrodes attached on each side. Strict conditions apply to the membranes which much be kept wet to allow proton conduction but should not be flooded either. Surplus water produced at the cathode should be pushed out of the stack to avoid blocking of the reactants diffusion. Besides, heat is produced from reaction 2.2 which should be evacuated to avoid overheating, causing damage to the membrane [33].

Hydrogen storage in canisters

Hydrogen is an interesting energy carrier because of its high specific energy, or energy per kg: 140 MJ/kg HHV or 120 MJ/kg LHV (Higher and Lower Heating Value respectively). The usage of HHV and LHV depends on the application's temperature. As the fuel cell used here operated below water's boiling point, HHV is preferred over LHV. The high energy density of hydrogen has motivated its usage as a fuel for space space missions [11]. However, H_2 has also a very low energy density, or energy per volume. This problem is usually solved by pressuring or using liquefaction techniques, in which more molecules are forced into a specified volume. However, these techniques are less relevant in the case of H_2 as its liquid density is low (71 kg.m $^{-3}$) and the liquefaction happens only at 22 K. This means a lot of energy has to be used in order to compress the hydrogen molecules, which does not weigh the advantages of such a process. Other methods to store the H_2 molecules have thus been sought, such as adsorption onto carbon materials, Metal Organic Frameworks or metal hydrides. The canisters used in this study use metal hydrides.

A metal hydride is a metal which has been bonded to hydrogen to form a new metal compound. The simplified reaction can be found in equation 2.3, where M is the metal used. In practice, the metal will be an alloy, chosen for its proton holding capacity. The alloy used in the canisters available for this experiment is rare-earth based, a so-called AB5 type of alloy. The advantage of such alloy is the high hydrogen absorbtion capacity combined with a moderate range of operation temperatures (up to 60° C). An example of rare-earth alloy is: $La_{10.5}Ce_{4.3}Pr_{0.5}Nd_{1.4}Ni_{60.0}Co_{12.7}Mn_{5.9}Al_{4.7}$ [34, 35].

$$M + H_2 \leftarrow MH_2 \tag{2.3}$$

Advantages of such bonding are numerous. First, the hydrogen molecules are densely packed in the regular lattice of the metal, instead of circulating freely and randomly as a gas or liquid (figure 2.3). Second, having the hydrogen in solid form makes the system safer in usage. H₂ gas is to be

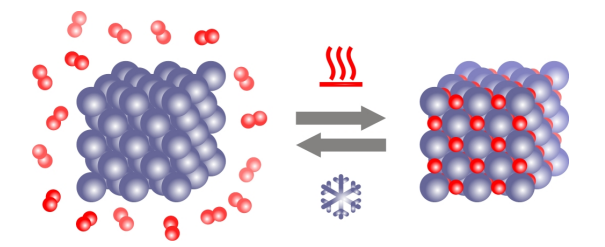


Figure 2.3: Working principle of a metal hydride: the cube of grey atoms represents the metal lattice. Each red dot is a hydrogen atom, which can be inserted into the voids of the metal structure. This process releases heat.

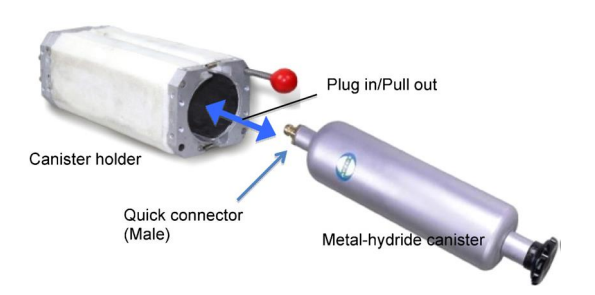


Figure 2.4: Metal hydride canister and its holder

handled with care because it has the lowest molecular weight of all gases. Hydrogen leaks faster than other gases, is flammable and highly volatile. However, this is also an advantage as the concentration level needed for ignition (4%) or detonation (18%) as less likely to be reached as any gas leak will disperse very quickly [11] (this benefit becomes a problem in indoor situations when the ceiling traps the hydrogen). Nevertheless, leakages should be avoided as much as possible, which is possible with a metal hydride canister.

Being fueled, the metal alloy absorbs hydrogen molecules, creating new bonds with the structure. This process is exothermic, and should thus be cooled. Once full, the canister can go to the end-user, who is going to click it into his scooter (figure 2.4). The desorption mechanism being endothermic, heat must be provided for the hydrogen to leave the canister. Hence the fuel will only leave its tank as soon as the motor of the vehicle is turned on and heat is circulated around the can. This initial heat is provided by the battery.

The maximum amount of hydrogen which can be provided by the two canisters used in this scooter is 90 g total. The mass of each canister is about 4275 g, making the weigh percentage fuel/holder 1%. The energy contained in 90 g of hydrogen is 3.5 kWh, which is approximately one third of the energy contained in 1 L gasoline.

There are 4 canisters used in this study. While two were in use, the other two were fueled in the lab charging station. This process is illustrated in figure 2.5: the canisters are clicked in a holder and connected through pipes to a hydrogen supply of 10 bar. Thanks to the quick connector system, the canisters are maintained vertically and are doused in a water bath which is maintained at 5°C. This cooling is necessary to maintain the adsorption process of the hydrogen molecules into the metal lattice. A flow-meter is used to monitor the flow rate of hydrogen into the canisters. As soon as the flow rate is zero, the canisters are full. The charging process took about 2 hours on average. Then, the

canisters are clicked out, set to rest until they reach ambient temperature again, and then weighed.



Figure 2.5: Fueling set-up in the lab

2.2.2. Battery components

Fuel cell scooters are not powered by their fuel cell exclusively. In order to reduce the size of the main power source, a peaking power device is integrated in the system. This is especially relevant for scooters as space is even more limited than for cars. The usage of a peaking power device reduces the costs of the fuel cell, which is higher as the size/capacity increases. The use of a peaking power device also allows to follow transient power demand which is more challenging using FCs as a result of stresses on the membrane.

As indicated by its name, the peaking power device is used in times of peak power demand. It is recharged from the fuel cell in times of low power demand. The combination of a power source and a peaking power battery makes the power supply system "hybrid".

Lithium-ion battery

The ZES 4.8 scooter used in this study works with a lithium-ion battery as peaking power device. The Li-ion cells use nickel cobalt manganese (NCM) chemistry, which is a combination known for its high energy density [36]. The nominal voltage of the battery pack is 24 V and its charge 20 Ah.

2.2.3. System configuration and control

The electric diagram circuit of the fuel cell hybrid electric scooter is illustrated in figure 2.6. The fuel cell and the battery are placed in parallel in the electric circuit. The hybrid strategy used here is called "combined hybrid": the secondary power supplier (the battery) can power the load while being charged simultaneously by the principal power supplier (the fuel cell stack). This strategy is chosen for its flexibility and because the peak power supply is the combined output of both power components. A charger board, or Battery Management System (BMS) allocates the power demand either to the battery or the fuel cell. A booster, or DC/DC converter steps up the voltage from 24 V to 48 V in order to meet the motor's requirement. The motor is a brushless DC motor, which has a good efficiency and lacks the need of an inverter. The output connection allows connection to loads or to the grid. This is done with an Anderson connector, which connects the output plug of the scooter to a load with a highly insulated and resistant cable.

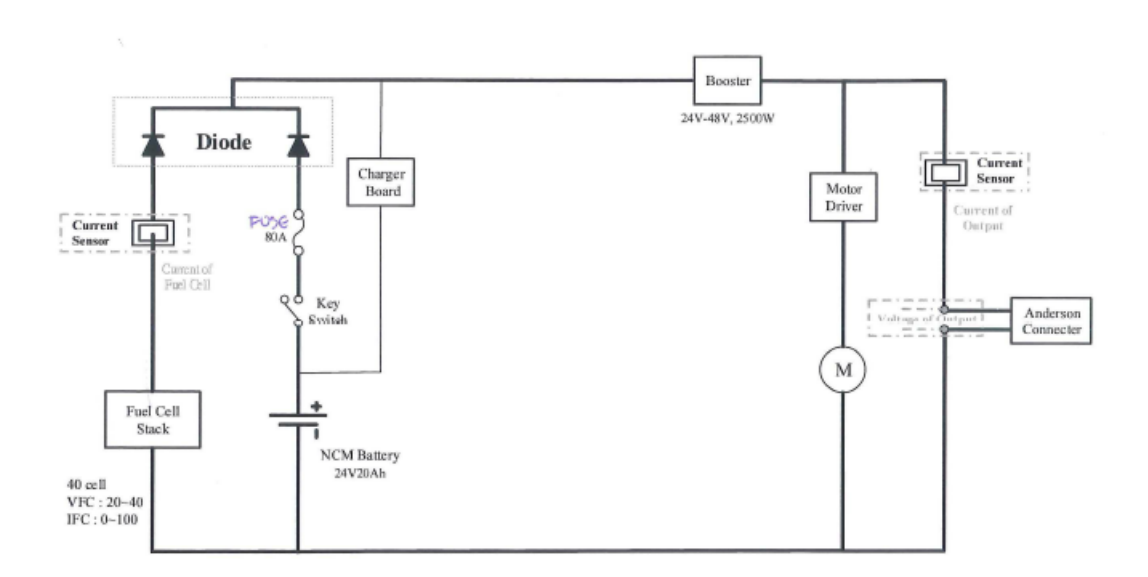


Figure 2.6: Electrical diagram of the main power components in the scooter and location of the current sensors installed

2.2.4. Balance of Plant

Besides the fuel cell and the battery components, there are also components which facilitate the power production. These are called the balance of plant (BoP). BoP components regroup all auxiliary equipment required to ensure the fuel cell operated as a reliable power source. These supporting components can be viewed in figure 2.7, where the general architecture of the scooter's system is depicted. Next paragraphs explain each of the subsystems (air, water and hydrogen) and the role of the BoP in maintaining the fuel cell stack's operation.

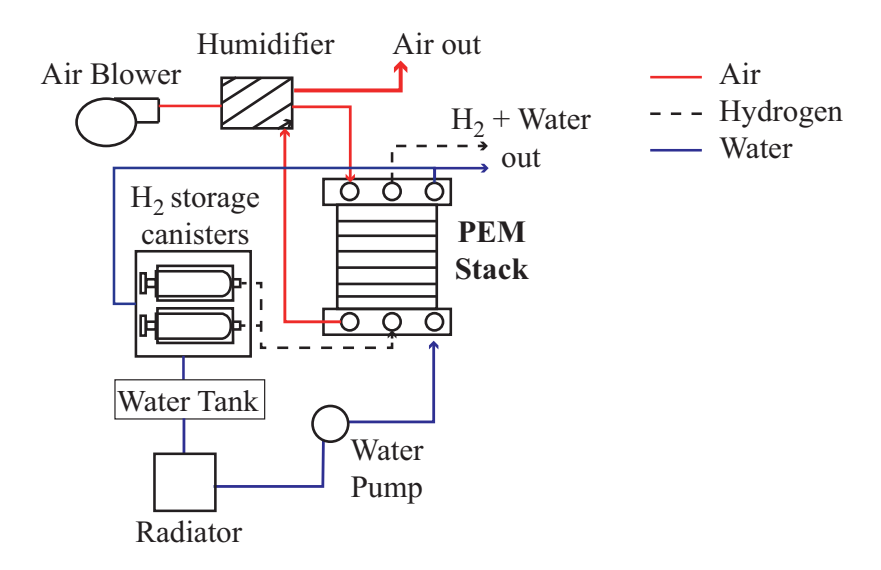


Figure 2.7: Architecture of the supply systems and BoP

The red arrows in 2.7 represent the air flown through the system. BoPs involved in this supplying air to the fuel cell are the air blower and the humidifier. The air blower feeds air from the surroundings into the scooter. The oxygen from the air is namely needed as the second reactant, besides hydrogen from the canisters, to drive the fuel cell. The humidifier provides heat and humidity to the incoming oxidant, which is critical for the overall system performance and reliability. Drying out of the fuel cell membrane can reduce the proton transfer and reduce the oxygen reduction reaction at the cathode. This leads to a poor fuel cell performance or even failure of the system. Two streams leave the humidifier, one air flow with the correct temperature humidity which is led into the fuel cell, another flow with the remaining air which is release into the surrounding atmosphere.

The blue arrows in 2.7 represent the water flow system of the scooter. Water is used as a coolant fluid to prevent excessive temperature rise from the fuel cell stack. Temperature is a critical parameter as it affects reaction kinetics, transport of water, humidity level and conductivity of the membrane. Controlling temperature is thus an important issue within a fuel cell system, and is facilitated here by the water pump, the radiator and an external fan (not depicted on figure 2.7). The pump drives water through the system at a given flow rate which cools the system. Excessive heat is lead into the radiator, which dissipates it out of the scooter system. The additional fan is at the front of the scooter, and starts blowing as soon as the cooling water and the radiator cannot keep up with the heat generated by the fuel cell reaction.

The black dashed arrows represent the flow of hydrogen. Hydrogen is leaving the canisters to enter the fuel cell stack. Once reacted at the cathode with the oxidant, hydrogen becomes water. The water coming out of the stack is partly directed to the canisters, to warm up the hydrogen and allow release. The rest of the water is released out of the system and discharged by a pipe. Some hydrogen is also led out of the system, especially when the fuel cell is purged. Hydrogen is then led through the stack at high pressure to remove any accumulated water and nitrogen which could jeopardize fuel cell stack performance.

2.3. Design of the duty cycles

Different duty cycles were designed to mimic actual driving, power delivery to the grid and patterns of electrical appliances. The next paragraphs will explain how each load pattern was defined.

2.3.1. Driving mode

The driving cycle applied to the FCES in this study was based on the Taipei Motorcycle Driving Cycle (TMDC), which has been developed with real-data use [37]. It is much closer to real-life driving than a theoretical driving cycle such as the ECE-40 for example [33]. However, since the constant power mode was used in the load and the maximum power that could be applied was 1 kW, some modifications were made to the original TMDC. The changes carried out are listed here.

- 1. The driving cycle was translated from velocity to instantaneous power demand using the physical model described in Lin's work [33]. A detailed explanation of the way the instantaneous power was derived can be found in A.
- 2. The power demand was truncated both at its lower and upper limit. The maximum power demand to drive the scooter was truncated from 1.6 kW to 1 kW, which is the maximum power deliverable by the electronic load. The minimum power demand was set to zero, out-cutting the negative power demand representing regenerative braking which our scooter was not able to provide.
- 3. The sharpness of the signal was smoothed out using a median filter in order to meet the electronic load's capability of changing power demand. Such a filter replaces each point in the signal with the median of adjacent points and has the advantage not to change significantly the signal if the duration of the spike is low.
- 4. A representative segment of the drive cycle was chosen and repeated to match the number of entries of the electronic load's software WAVY. A segment of 341 seconds was chosen to be repeated three times, yielding an experiment of 1024 seconds.

In figure 2.8, the different steps taken in the modification of the drive cycle are illustrated. Quantification of the changes can be found in table 2.2. The adjustments mostly affected the maximum power demand. The average and the maximum acceleration power staid more true to the original signal. In future work, a different electronic load could be chosen to increase the resemblance between the duty cycle applied to the scooter and the reality.

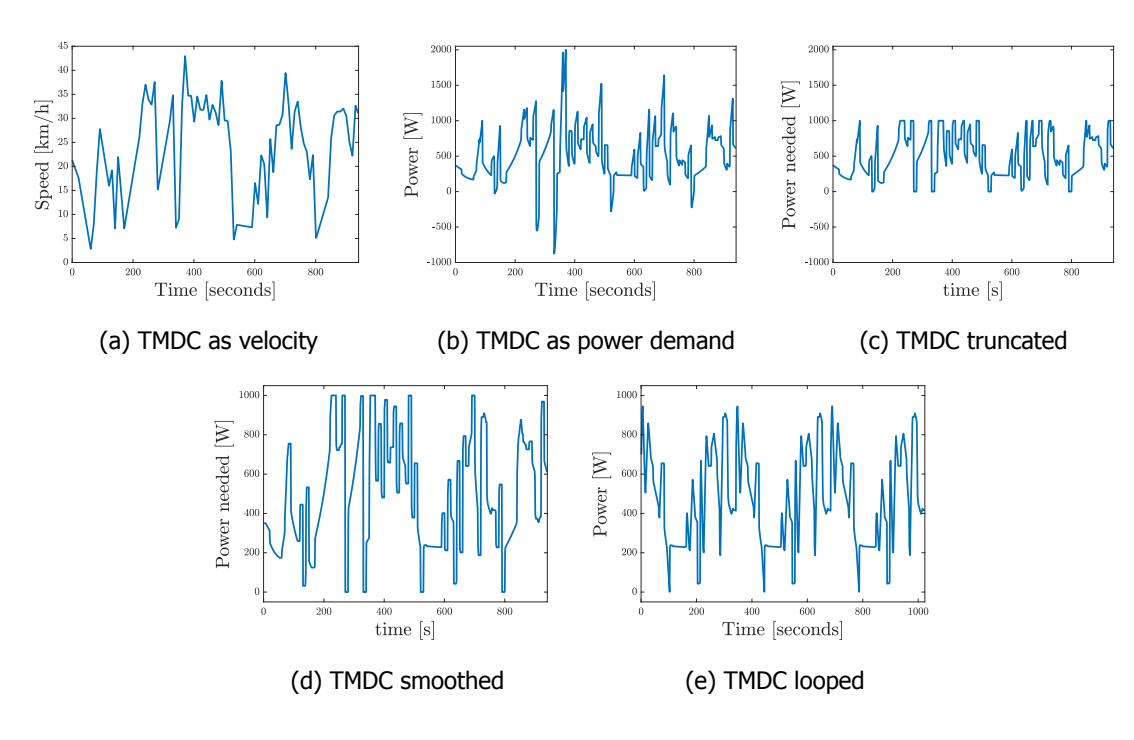


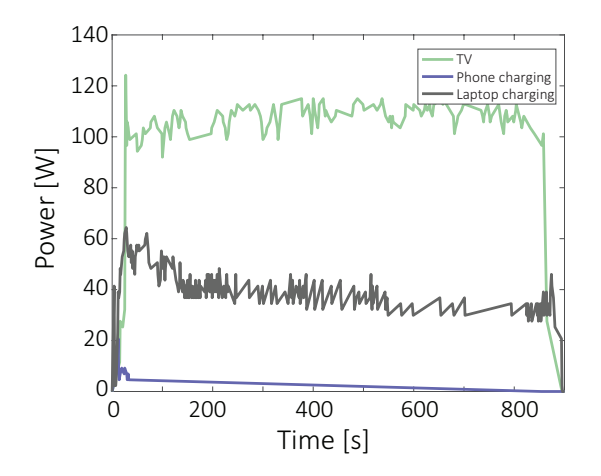
Figure 2.8: Steps in TMDC modification

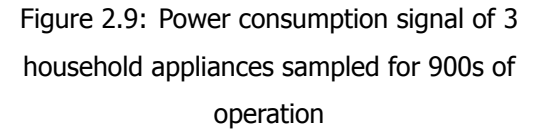
Table 2.2: Characteristics of the original and modified TMDC

	Original TMDC	Modified TMDC	% change
Average velocity [km/h]	24.8		
Max net power [W]	1999.4	944.6	53
Average power [W]	519.7	446.7	14
Max acceleration power [W]	718.9	566.3	21

2.3.2. Vehicle-to-Load mode

The duty cycle for V2L was designed using real consumption data of appliances, measured using the Voltcraft Energy Logger 4000. Resistive loads, i.e. those containing a heating element, such as microwaves, coffee machines or bread toasters were excluded because the high initial spike of instantaneous power demand exceeds the maximum load power that can be dealt with by both the electronic load and the scooter [38]. Therefore, these appliances were identified as non-suitable for V2L applications for the scooter. The juxtaposed signals of 2 mobile phones, 2 laptops and one television were chosen as duty cycle for V2L. The individual signal per appliance is shown in 2.9. As explained in section 2.3.1, it is not possible for the electronic load to deliver power for more than 256 different pre-programmed entries. Therefore, it was chosen to take one piece of signal of 256 entries and repeat it four times, for a length of experiment of 1024 seconds. The final V2L duty cycle can be viewed in 2.10.





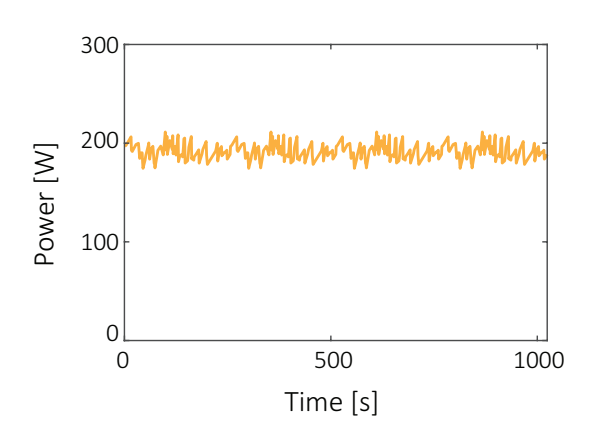


Figure 2.10: Final V2L duty cycle designed to match the characteristics of the electronic load

2.3.3. Vehicle-to-Grid mode

To mimic the use of the scooter for V2G application, it has been chosen to submit it to a constant power demand of 1 kW. This was the maximum power demand possible in this setup, which was limited by the DC load. It is close to the scooter's maximum V2G capacity of 1.2 kW. In future applications for V2G, this maximum value of 1.2 kW electric power delivery might be used. If scooters are aggregated with the purpose of providing the grid with frequency reserves, much power will be needed, hence the scooters will be run on maximal capacity.

2.3.4. Comparison of the duty cycles

The three duty cycles defined here above are illustrated in figure 2.11. Each of them is very different in terms of type of power demand (transient vs constant) and in terms of power demand range. Figure 2.12 illustrates the load duration curves per mode, where the percentage of time each power level is delivered is shown. The drive and load cycles are fairly constant demands while the drive cycle requires a broad range of power levels.

2.4. Experimental procedure

The scooter was driven 3122 km in Taiwan before performing the experiments. Data on this usage was not recorded and thus the degradation process undergone before the start of the experiments is not known. The duty cycle patterns were uploaded into the software WAVY, which submitted them to the electronic load Kikusui PLZ4-1000W via a USB connection. The electronic load was itself connected to the scooter via the Anderson connector, as shown in figure 2.13. In this way, DC power was supplied from the scooter to the load.

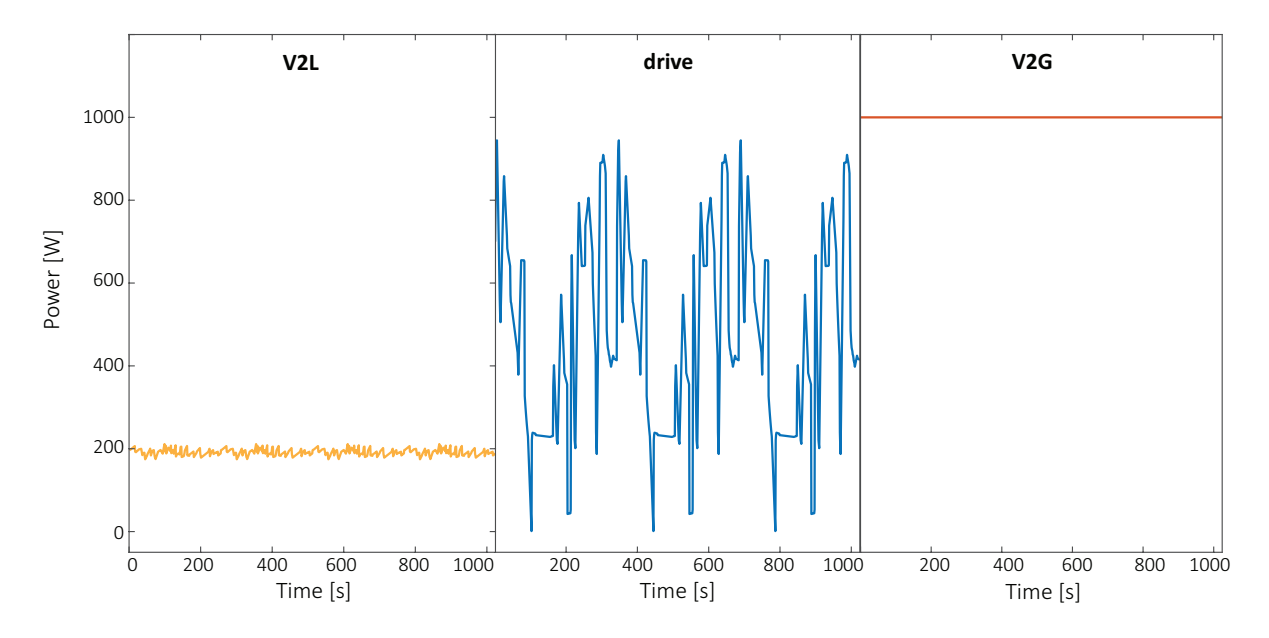


Figure 2.11: Duty cycle designed per mode

Each of the designed duty cycles was submitted 30 times to the FCES in random order, which makes 90 runs in total when accounting for the three modes. The experiments were performed in the fuel cell lab of the TU Delft over a period of 3 months. The order and date of the experiment can be found in the appendix B.

The scooter was warmed up to at least 30 °C before the start of the duty cycle in order to make the experiments more comparable. Between each experiment, we waited until the scooter was cooled down close to its starting temperature. Each test was performed as follows: the data-logger was turned on, then the scooter and finally the electronic load. The load applied a duty cycle to the scooter for 1024 seconds. After the load was turned off, the scooter was shut down and finally the data-logger. This is schematically illustrated in figure 2.14. The idling time denotes the time when the scooter was ON, but no load was applied. Measurements of the variables during idling time were also performed.

Sensors were installed in the scooter to measure the current and voltage of resp. the fuel cell, the battery and the output delivered to the load, the temperature of the fuel cell and the canister, the pressure and the mass of hydrogen within the canister. These variables were measured with a sample frequency of 1 Hz and stored in the data logger Hioki LR841. Calibration curves for the sensors can be found in appendix C.

To construct the polarization curves, a constant current was applied to the FCES for 2 min, and was each time increased by 1 A. The set range of currents was between 1 and 20 A, above which the battery was known to deliver the additional current to the load. The current measured at the FC

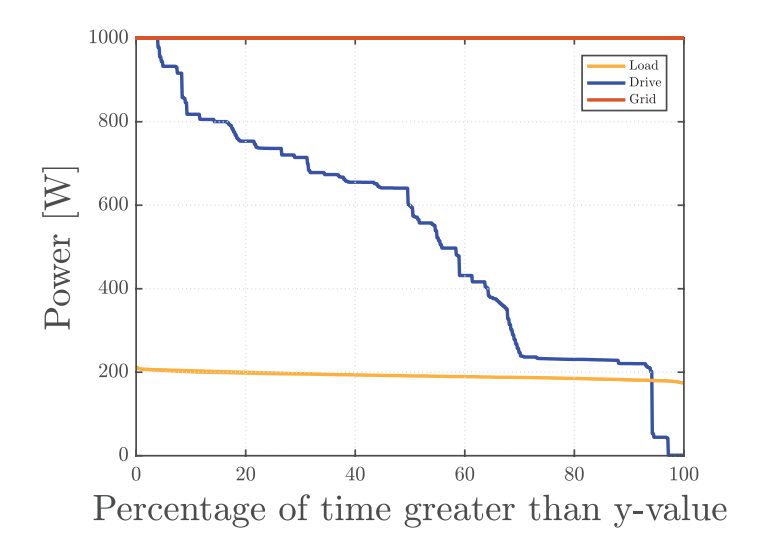


Figure 2.12: Load duration curve for each mode

is different than the set current because of the share taken by the battery. In order to get the most representative FC current/voltage couple, the average value of the last 30 seconds of each current plateau was taken for the elaboration of the IV curve: during the 2 min of applying a current, the voltage needs to stabilize beyond its transient behaviour.

2.5. Data analysis

92160 data entries per variable came forth from performing the experiment, as 1024 measurements were done per run, with 30 runs per mode. The different data analysis methods used to translate the raw data from the experiments into useful information to answer the main research question are outlined here.

First, a descriptive analysis was performed to explain the general behaviour of the variables in each of the modes. The distribution of the data is displayed in boxplots, showing the minimum, maximum, first, second (median) and third quartiles of each variable per mode. Each boxplot is the graphical representation of 30 data-points.

Then, a Principal Component Analysis was performed in order to compare the different modes of operation of the scooter and find the variables accounting most for these differences. This statistical tool helps finding patterns in high dimensional data-sets by prioritizing variables which account for a large part of the data spread. The size of the data-set is compressed as only the Principal Components (PCs) are kept. These PCs are obtained via linear combination of the original variables. This method has already shown to be effective in analyzing fuel cell data [39]. The average for each variable and

2.5. Data analysis



Figure 2.13: Connection cable between the scooter and the electronic load

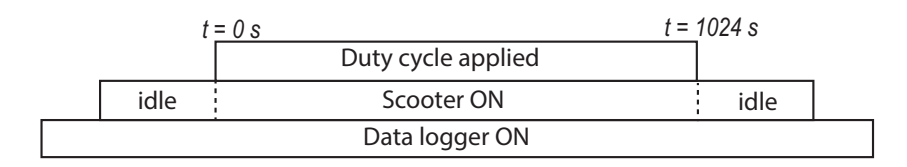


Figure 2.14: Schematic view of the course of an experiment

repetition was taken to perform this PCA analysis in view of generating a clear output.

Finally, a empirical model was constructed from a linear regression analysis to determine which mode led to the most significant drop in fuel cell voltage. FC voltage drop was predicted per mode by the respective regressors time and FC current. All data analysis was performed in Infostat statistical software.

3

Results

By applying the different duty cycles described in section 2.3 to the scooter, the functioning of the system can be assessed and the fuel cell performance degradation can be analyzed. In this chapter, the analysis of the system's behaviour is performed. The general dynamics of the power system are described using the average instantaneous power share between fuel cell and battery. An exploratory variable analysis is performed using boxplots. The hydrogen consumption and the efficiency of the system is assessed in each mode. The variables weighing most in differentiating the modes are highlighted in a PCA analysis. Finally, the voltage drop is analyzed as a function of time and of current.

3.1. Operation of the power system in the different mode

3.1.1. Power dynamics

The general dynamics of the power system are best described by the power output of each power component, fuel cell and battery. Figure 3.1 depicts on average over the 30 runs the power output as well as the respective shares taken by the fuel cell and the battery in delivering this power demand. A brief interpretation of the figure is given per mode.

V2G

In the Vehicle-to-Grid mode, the power system must output 1 kW every second. Both fuel cell and battery are needed to supply this power demand, in varying shares along the 1024 seconds experiment. The fuel cell handles the largest part of this demand, with an increasing share from 650 W to 1 kW. The battery is providing more power at the start, until the FC is warm enough for a higher output.

26 3. Results

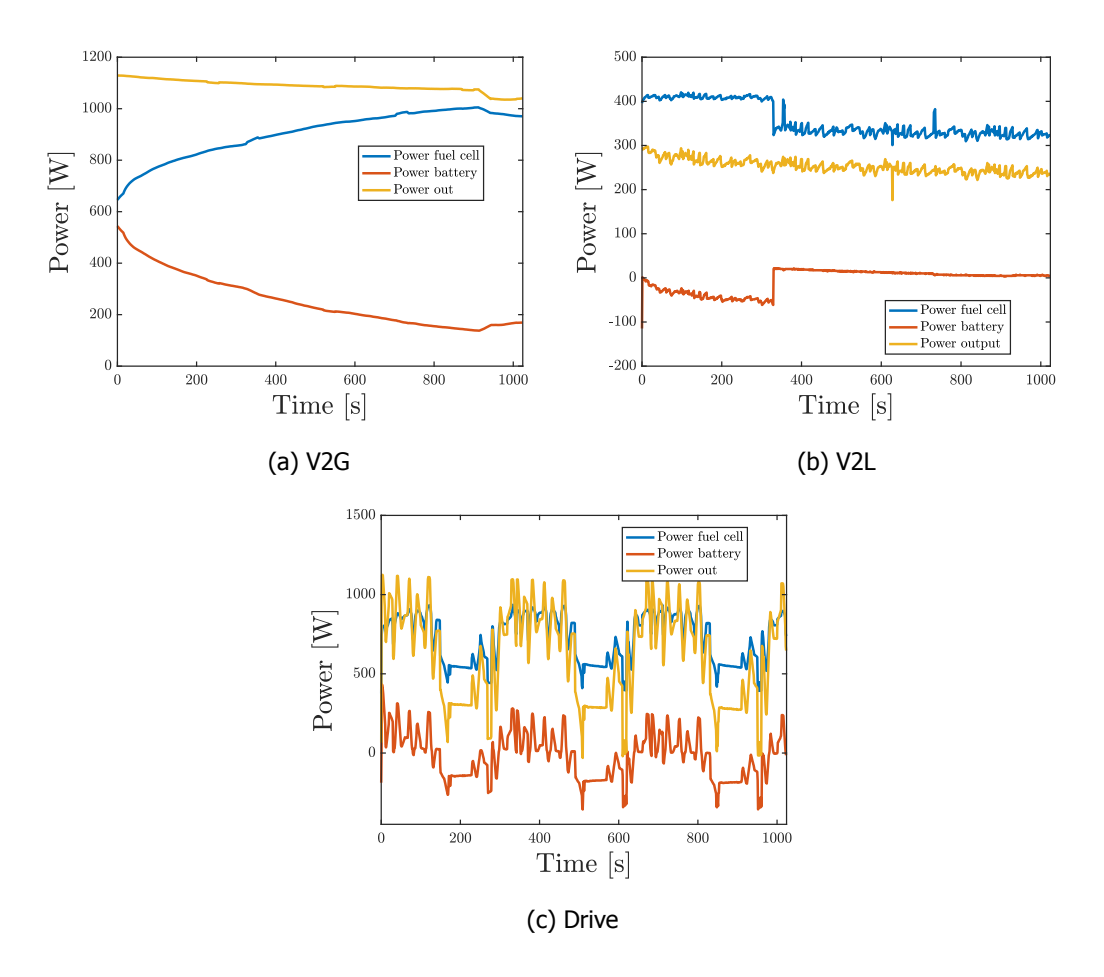


Figure 3.1: Energy management for a typical duty cycle, per type of experiment

V2L

In the vehicle-to-Load mode, the power demand is always lower than the fuel cell limiting-power point. Moreover, the temperature is not limiting for the fuel cell to deliver the power demand: the demand is low, such that the FC temperature needed for such a power demand is reached immediately. Consequently, the battery is not necessary in V2L mode for power delivery and can either charge (P_{batt} < 0) or stay stand-by (P_{batt} = 0). In figure 3.1b, the battery is being charged until t = 360 seconds, after which the battery is set to stand-by. To charge the battery, the fuel cell needs to provide approximately 70 W additional power. The power allocation pattern shown in figure 3.1b corresponds to the average pattern encountered throughout the 30 V2L runs. In fact, three types of V2L energy management patterns were found:

- 1. the battery is charging throughout the whole run,
- 2. the battery is by-passed throughout the whole run,
- 3. the battery is first being charged, then by-passed.

The V2L energy management patterns for all runs can be found in appendix D. The different manage-

ment strategies can be related to the state-of-charge of the battery.

Driving mode

The driving mode has a variable power demand, which mirrors the TMDC. Figure 3.1c shows the role of the battery and the fuel cell in providing this transient power demand. The battery is alternatively being charged and discharged during a drive event. From there, the FC limiting point can be determined: the battery kicks in as a power source when the power at the output is higher that 600 W. Below this limit, the battery is not necessary as a power source and has the possibility to recharge. Similarly to the other modes, the fuel cell accounts for the largest share of overall power generation, with an average power delivery above 500 W throughout the drive cycle. The battery supplies the power needed above the FC limiting point. Moreover, the battery takes care of the sharpest power changes. While the power delivered by the fuel cell is a rounded approximation of the power demand, the power delivered by the battery follows the peaky pattern of the power demand. The sharpness of the peaks reflects the variability in power delivered and can be quantified using power gradient $\frac{dP}{dt}$ or power change in time. As a comparison, the average positive and negative power gradients delivered by the fuel cell are resp. 17.1 and -14.9 W/s while the battery delivers average power gradients of 22.7 and -17.4 W/s. A choice has been made in the energy management system to relieve the fuel cell from excessive transient loading.

3.1.2. Distribution of variables per mode

From the average power component operation, we now move to the distribution of all the data acquired in the tests per variable and per mode. An exploratory data analysis was performed for each variable measured throughout the experiments. Figure 3.2 displays boxplots of each variable per mode.

For both the fuel cell and the battery, the V2G mode was characterized by higher current values and lower voltage values. Both power components can be viewed as a generator, with an internal resistance to which Ohm's law applies: $R_{int} = \frac{V_{FC}}{I_{FC}}$. When the fuel cell generates more power, the current increases, meaning the voltage has to decrease to keep the resistance constant. The fuel cell was producing most power in V2G, hence the highest fuel cell current values of the three modes. As more power is generated in V2G events, more heat is generated too. The temperature of the fuel cell rises to higher levels, up to 57°C for V2G. The drive mode has a wider range of fuel cell current values: the power demand and thus current were very variable throughout a run. As to the fuel cell voltage, the largest spreading is observed for V2L tests, which is due to the varying amount of power the fuel cell delivers: when the battery is being charged, the fuel cell has to compensate the latter's power consumption by producing more.

The battery current is highest for the V2G mode. Over 75% of the battery current values are pos-

28 3. Results

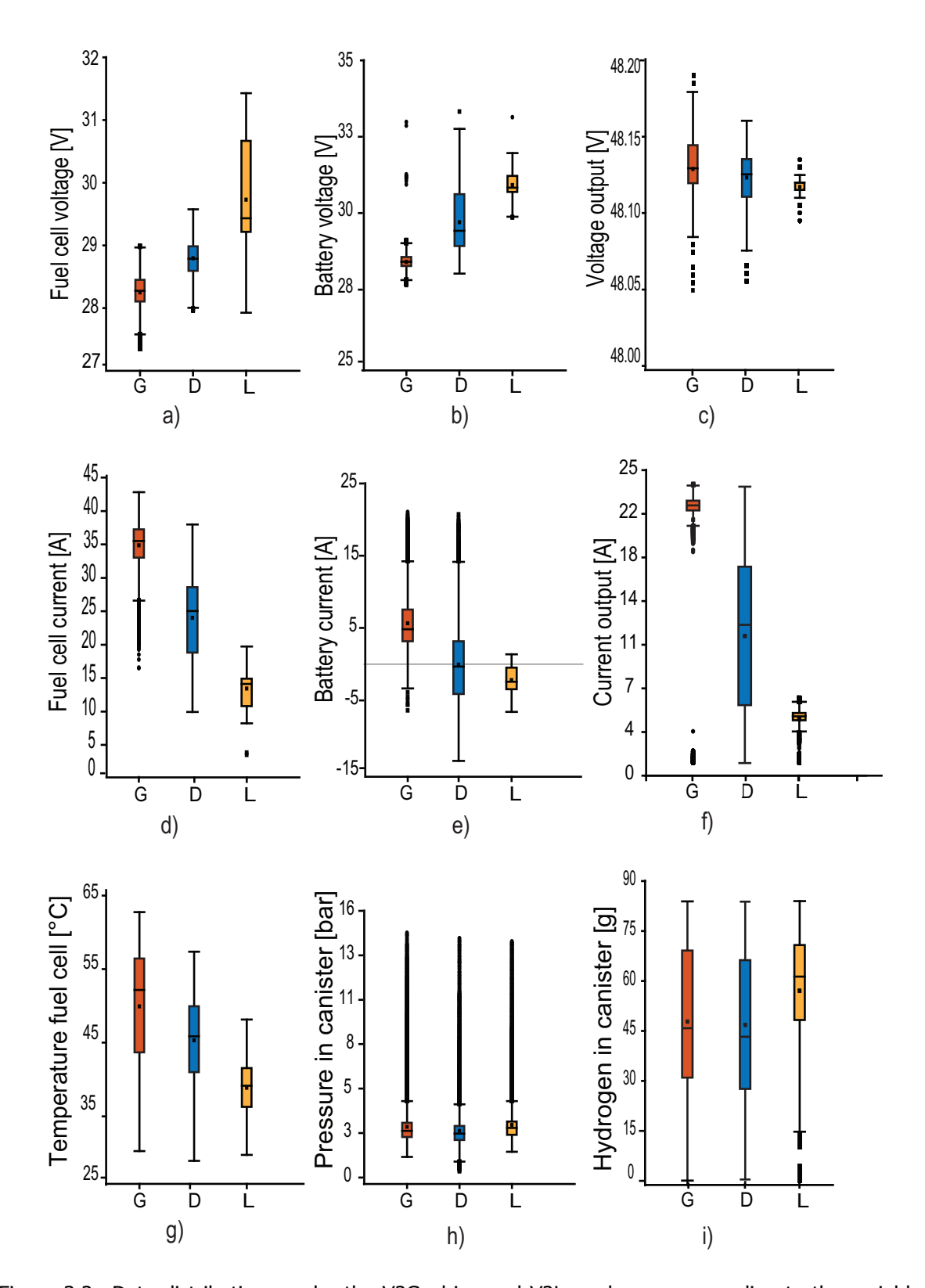


Figure 3.2: Data distributions under the V2G, drive and V2L modes, corresponding to the variables a) FC voltage, b) battery voltage and c) output voltage, d) FC current, e) battery current, f) output current, g) temperature of the FC, h) pressure within the canisters, i) mass of hydrogen present in the canisters. Central points within the boxplots represent the average value; boxes mark the 25th and 75th percentiles and the segment within the box represents the median; segments outside the box mark the values that extend 1.5 times the width of the box; points outside are outliers.

itive, which reflects the fact that the battery is delivering power to support the fuel cell. In the other modes, the battery is operating more dynamically, being either charged or discharged throughout a run. In the drive mode, the battery is evenly being charged and discharged, while it is mainly being charged in the V2L mode. The voltage of the battery is governed by its state, charging or discharging. When discharging, the battery voltage is lower, as it is the case for V2G. When charging, higher potential is needed to drive the reverse reaction. This is why the voltage of the battery in V2L events is much higher than for V2G events. It must be noticed that all voltages from the battery are far above the nominal voltage 24 V, which is the voltage at which the battery is designed to operate. This induces a faster degradation.

The output voltage is fairly constant independently of the mode. For each mode, the average V_{out} is comprised between 48.10 and 48.15. This is regulated by the DC/DC connector, which ensures constant output voltage to enable connection with the grid, motor and load. The V2L case is the most constant one, probably because the battery is never supplying power out, and that it is easier to regulate one over two power components' voltage output. The output current is proportional to the output power demand, with I_{out} being the highest for V2G, then drive and last V2L. The range of data is also representative of how variable the power/current demand is. V2G and V2L events have fairly constant power demands, while the varying driving cycle make I_{out} for driving tests occur in a wide window of possibilities.

There seem to be no major difference between canister pressure among modes. The average canister pressure is around 3 bars, with many outliers above the 5 bar. The pressure is essentially a function of the amount of hydrogen contained in the canister, which is varying similarly among the 3 modes. The mass of hydrogen varies between the maximum containable mass 90 g and an empty set of canisters 0 g. Most of the measurements were performed in the mid to high level of fuel. Indeed, canisters were replaced before the event not to run out of fuel during an experiment. V2G and drive runs were performed in a bigger range of hydrogen mass in the canister, as more hydrogen was consumed throughout these experiments. Less energy and thus less hydrogen was demanded in V2L mode, such that the canisters were depleted less throughout a run.

3.2. Balance of plant components

In order to gain insight in the scooter system as a whole, parasitic power consumption from the Balance of Plant (BoP) components needs to be taken into account. As explained in chapter 2, the BoP of our fuel cell includes as three main components:

- 1. The air blower, which pushes air from outside inside the FC as a fuel for cathode;
- 2. The cooling pump, pumping water around the system in order to dissipate the heat from the FC

30 3. Results

into the radiator;

3. The fan, which blows any additional heat onto the radiator.

The individual share of each BoP component is not measured throughout the experiments. The total BoP per second is known from equation 3.2. There, we assume all power which is produced but not harvested at the output is to be consumed for the BoP.

$$BoP = P_{FC} + P_{batt} - P_{out}$$
 when $Pbatt > 0$ (3.1)

$$BoP = P_{FC} - P_{out}$$
 when $Pbatt < 0$ (3.2)

Now it is interesting to understand what this energy is used for, and try to unravel how the BoP is shared among components. From Lin, the share of the individual BoP components to constitute the total BoP is as follows: the blower accounts for up to 80% of the BoP when used at maximal flow rate, the coolant pump for 10% and the fan blowing over the radiator 10% [33]. In his work, Lin takes the blower power consumption to be linearly dependent on the power demand. Indeed, larger systems have their FC optimized with a good fuel feed stoichiometry ratio and thus a varying air blower. However, in small systems like the scooter, the air blower just feeds in a constant, maximal amount of oxygen. A constant power demand of 60 W is allocated to the blower and the coolant pump combined.

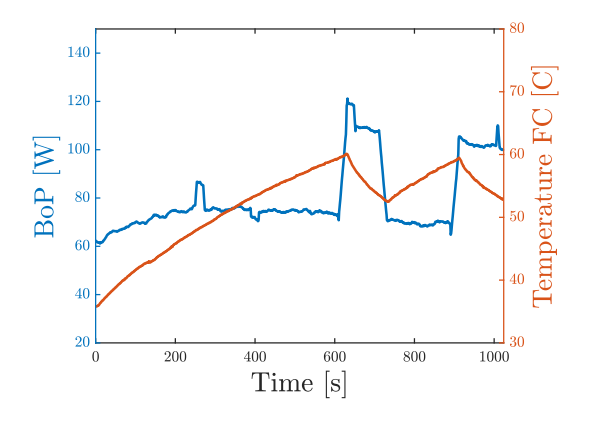


Figure 3.3: Effect of the fan on BoP power consumption and temperature of the FC in a V2G experiment

Figure 3.4: Power delivered by FC as a function of temperature

Besides, the use of the fan at higher temperatures leads to an increased BoP. Looking at the fuel cell performance throughout the test, its optimal temperature is comprised between 50 and 60°C. As soon as the temperature of the FC reaches 60°C, the cooling fan turns on, which makes the BoP increase from 60 to 100 W. This can be seen in the grid experiment depicted in 3.3. Figure 3.4 shows the power delivered by the battery as a function of temperature. The V2L events can be performed by the FC right from the start, the FC can output 300 W even at ambient temperatures. However, the V2G events

show that the FC needs to be warmed up to 50°C approximately in order to provide power of 1 kW and higher.

3.3. System efficiency

Now the different modes of operation are compared in terms of efficiency. The scooter has only the hydrogen canisters as energy source, there is no external plug-in for battery charging. Consequently, the efficiency of the hybrid system is calculated considering the power from the fuel cell alone.

$$\eta_{syst} = \frac{E_{out} - \Delta E_{batt}}{E_{H_2}} \tag{3.3}$$

The efficiency of the hybrid system is defined in equation 3.3, where the energy output E_{out} is the energy delivered as duty cycle, ΔE_{batt} is the difference in battery energy and E_{H_2} is the energy contained in hydrogen. The nominator is the energy delivered by the fuel cell, while the denominator is the energy input into the fuel cell. The output energy, or electric energy delivered to the load, is defined as the average $\int P_{out} dt$ per load. ΔE_{batt} is the difference between the energy discharged by the battery ($E_{batt,dis}$) and the energy supplied from the fuel cell to charge it ($E_{batt,ch}$), as shown in equation 3.4.

$$\Delta E_{batt} = E_{batt.dis} - E_{batt.ch} \tag{3.4}$$

Correcting for the battery charging throughout a mode is important to be able to compare fairly the efficiency. In each mode, very different shares of the power from the fuel cell are directed to the battery, as shown in the IV curve of the battery (figure 3.5). The battery is mainly charging during load events (I_{batt} <0), which means the H_2 consumption will be higher than indicated in the energy output. Similarly, the power delivered in grid events is produced partly by the FC (and thus the H_2 fed in) and partly by the battery, which drives on H_2 that was fed in before that event. The hydrogen consumption will thus appear to be lower than the atcual energy output. To correct for this, we subtract the change in energy content of the battery from the energy output.

The hydrogen energy E_{H_2} is calculated by multiplying the average hydrogen consumption during a test with the HHV of H_2 (142 kJ/g) as shown in equation 3.5.

$$E_{H2} = \Delta m_{H2} x H H V \tag{3.5}$$

 m_{H2} is the average hydrogen consumption of a mode. It was calculated by measuring the mass of the canisters before and after a series of 20 experiments. The measured mass differences included the hydrogen consumed during idling time. To account for this, the hydrogen consumed for idling was corrected: the time idling for each experiment being known, the average hydrogen consumption per

32 3. Results

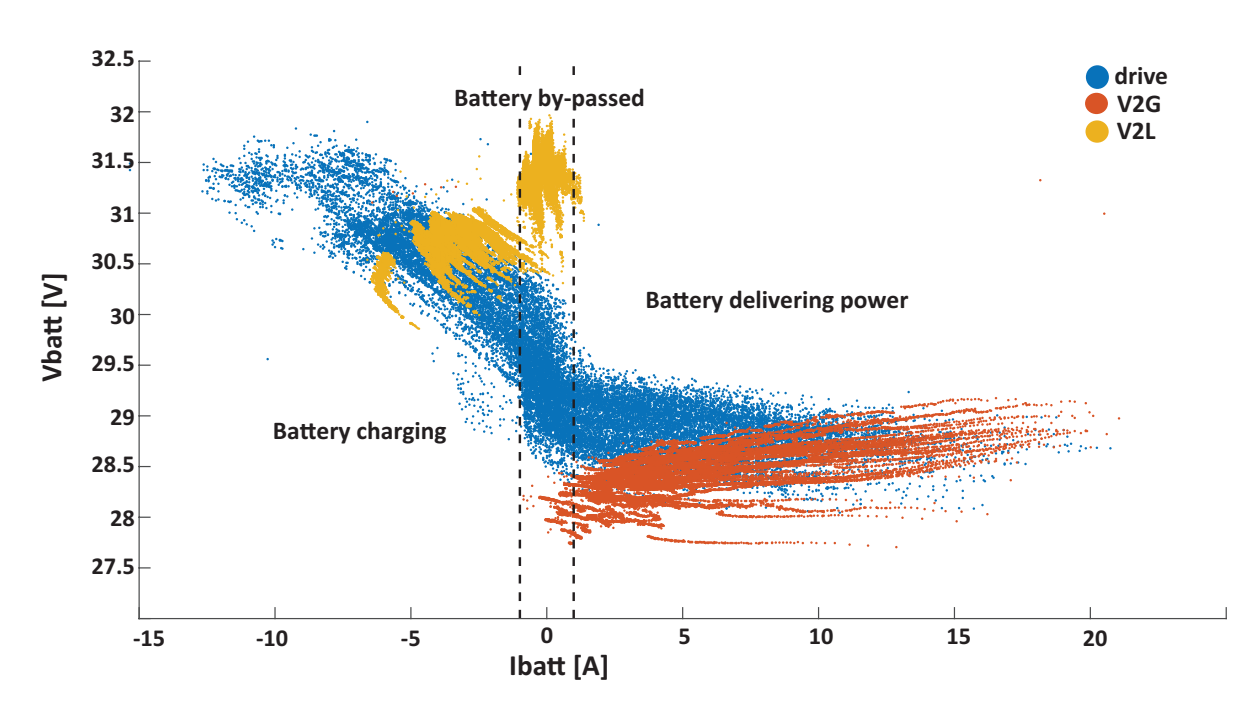


Figure 3.5: IV curve battery

Table 3.1: Average value for the consumed hydrogen and system efficiency per mode

Hydrogen consumption [g]	System efficiency [%]	
	HHV	LHV
13.8	32.0	37.8
16.8	39.4	46.6
7.6	29.2	34.5
	13.8 16.8	13.8 32.0 16.8 39.4

second idling was subtracted from the measured H_2 mass difference. More details on these computations can be found in Appendix C.

The efficiency of the system is highly dependent on the mass of hydrogen consumed throughout an experiment. Different approaches to compute these average hydrogen consumption values are compared in appendix C and the method with least inaccuracies was chosen. However, the mean hydrogen consumption values of the samples are not necessarily a good estimate for the real mean of the experiments. The means were computed using a sample of 6-7 measurements of hydrogen consumption per mode. These sample values of the hydrogen consumption measured (and corrected for idling time) are displayed in table 3.2. Some descriptive statistics to evaluate the data are added. SD stands for standard deviation, and is a measure of the variability of the data. The SD is relatively high, especially for the V2L events. The data is widely scattered. The standard error (SE) gives a measure of how uncertain the estimate of the means are. Again, it appears that the mean consumption of hydrogen in V2L is the most uncertain. From statistics, we know that 95% of the values are within 1.96x SE at

Table 3.2: Distribution and descriptive statistics of the hydrogen consumption values [g H2]

	Drive	V2L	V2G
Measurement values	15.51	7.09	16.19
	11.77	8.91	18.82
	13.18	11.06	15.76
	14.51	8.22	17.77
	14.58	6.92	19.13
	13.18	6.17	15.11
		4.61	14.90
Mean	13.79	7.57	16.81
SD	1.34	2.07	1.75
SE	0.55	0.78	0.66

either sides of the mean. This means that the hydrogen consumption in V2L mode is between 6.04 and 9.10 g, which represents a 30% uncertainty. This broad range of uncertainty is possibly caused by the differences between runs of the V2L mode: while the battery was being charged constantly throughout one run, it was by-passed throughout another one, or it was charged and then by-passed. Such variation in battery state was not controlled and might have led to a larger range of uncertainties in the mean estimated mass of hydrogen consumed. In future work, more measurements on the mass of hydrogen consumed during experiments could be performed in order to improve these estimates.

3.4. Ordination of the modes according to the variables

Principal component analysis (PCA) was used to extract the most important information from the variables measured in the experiments. Clear differences between the modes are identified using this method.

The results are shown in a biplot in figure 3.6. This type of plot is a combination of a scatter plot of the observations represented by dots, and another scatter plot representing each variable by vector line. Such a plot helps identifying in one glance the relationship between all variables and differentiating between the modes of the scooter.

The PCA is performed by taking the mean value of the variables for each run, yielding 90 points in a biplot graph. This choice is motivated by the fact that the global behavior between modes is assessed more than the intra-run behavior. Moreover, this PCA is performed using a select group of variables among the original set of measured variables. The temperature of the canister was left out because it

3. Results

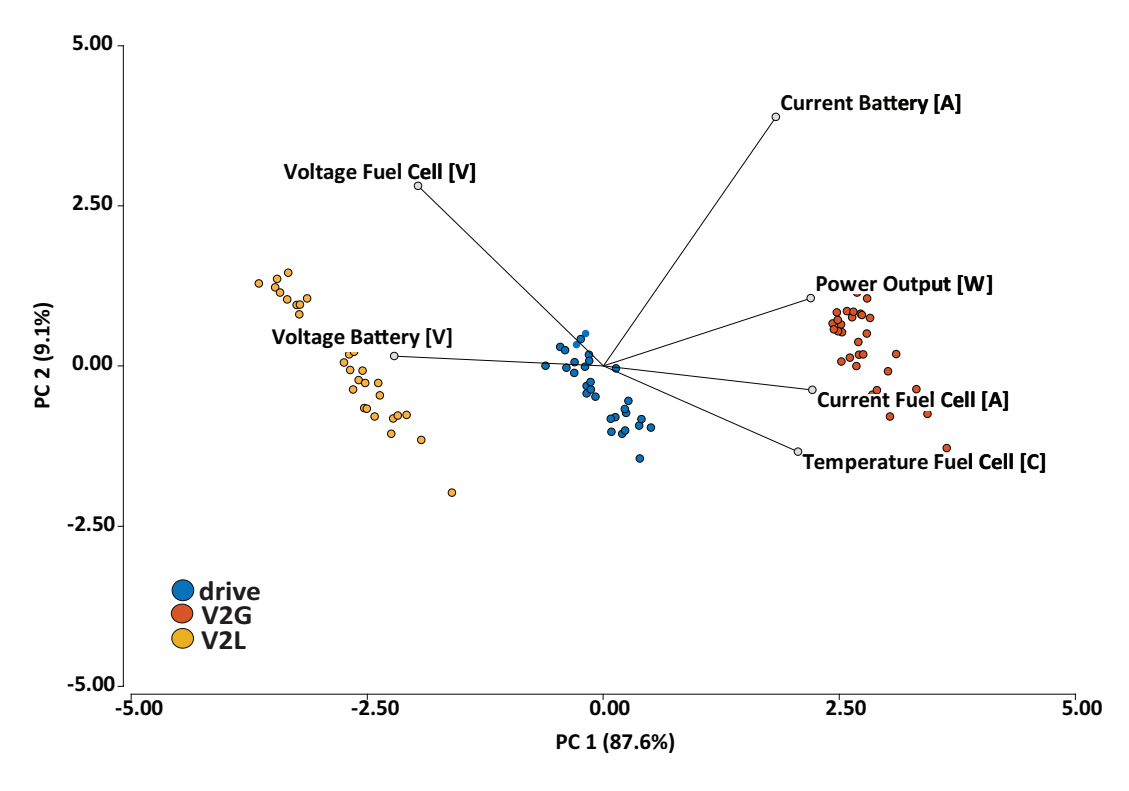


Figure 3.6: PCA results

shows almost exactly the same results as the temperature of the fuel cell. These variables are highly correlated. The output voltage and current was combined into one variable: the output power. The mass and pressure of hydrogen within the canisters were discarded in this analysis because of the lack of knowledge of the exact values per run. Indeed, a rough estimate of the hydrogen consumption was made but the values of hydrogen content per run were estimated not accurate enough to include here. Finally, the experiments were performed in random order which allows discarding the cumulative time of experiments. In the end, a simplified but clearer PCA was performed.

The axes of figure 3.6 show the two principal components. Together, they account for 96.7% of the total variability of the data. In figure 3.7, the increasingly explained variance is depicted per principal component. Using more than two PCs does not increase significantly the explanation of the data. Therefore, it has been chosen to work with a 2D plot showing only the first two PCs.

Figure 3.6 displays a group-wise distribution of the observation dots along PC1. Each group of one colour represents a mode, from left to right: V2L, drive and V2G. From this separation, it can be concluded that there is clear difference in variables per mode along the first principal component. Most variable vectors show a clear elongation on the first PC axis.

A separation between fuel cell and battery voltage from the other variables is observed along the PC1 axis. This means that the variability among modes can be explained by these variables. Indeed,

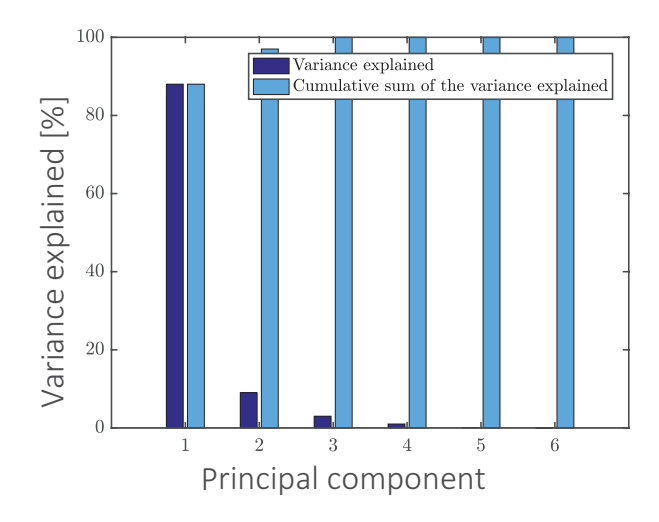


Figure 3.7: Variance of the data explained per principal components

Table 3.3: Eigenvectors of each variables per PC

Variables	PC1	PC2
Current Fuel Cell [A]	0.43	-0.07
Voltage Fuel Cell [V]	-0.38	0.55
Temperature Fuel Cell [°C]	0.40	-0.26
Current Battery [A]	0.36	0.76
Voltage Battery [V]	-0.43	0.03
Power Output [W]	0.43	0.21

the voltage between modes varies because of the different power demands. As the power demand is higher for V2G experiments, the currents of both the battery and the fuel cell are high in this mode. Consequently, a lower voltage is observed. An exact opposite situation is found for V2L experiments: low power yields low current and thus high voltage. The driving mode is situated in between the other two modes.

The fuel cell voltage and the battery current account for most variation on the PC2 axis: their eigenvectors have the highest magnitude, as seen in table 3.3. However, there is no distinction between modes on this principal component: each group of points is clearly aligned along the PC1 axis and not the PC2 axis.

3.5. Fuel cell degradation rates

3.5.1. Overall voltage decline rate

The PEM fuel cell degradation is a complex process which depends on numerous mechanisms. Separating the effect of each mechanism on the degradation process is a difficult operation, especially in

36 3. Results

real-life studies where conditions are less controlled than when studying individual fuel cells. Nonetheless, a general idea of the degradation can be formed using for example the voltage drop per hour and per cell, also called degradation rate. This parameter is thus often used in fuel cell degradation studies.

The degradation rate is obtained using a linear regression model, in which the fuel cell voltage is fitted against the time of experiment, as expressed in equation 3.6.

$$V_{fuelcell} = \beta 0 + \beta 1 * t_{experiment}$$
 (3.6)

By time of experiment, we mean the cumulative amount of seconds of experiments, including idling. Idling time is included here because it is thought to influence as well the fuel cell voltage drop. This regression is fitted throughout each second of all the experiments, without distinction of mode.

Table 3.4: Regression coefficients for fuel cell voltage modelled as a function of cumulative time without distinction of mode

Coef	Est.	S.E.	p-value
β0	29.21	0.01	<0.0001
β1 [V/s]	-4.50E-06	8.20E-08	< 0.0001
β 1 [μ V/h.cell]	-405		

The results of the linear regression model can be found in table 3.4. The intercept $\beta 0$ indicates the fuel cell voltage at the start of the experiments. The slope $\beta 1$ is a measure of the overall fuel cell voltage change during the experiments. The resulting voltage change is negative, which hints for fuel cell degradation. Translating the raw values of the fuel cell degradation rate from V/s for the whole FC stack to μ V/h per cell yields an overall degradation rate of 405 μ V/h.cell when the scooter is operated alternatively in the different modes. Both the intercept and the slope of the empirical regression model are statistically significant, with p-values below 0.0001. The standard error values are small, indicating an accurate model to represent the voltage/time relationship.

An overall degradation rate of 405 μ V/h.cell is high, and should therefore be related to other studies. This is however difficult as most studies focus on the degradation of a single cell or a stack in strictly controlled conditions. In this study, the fuel cell system was part of a more complex hybrid system, interacting with a battery. Moreover, as the FCS was inside the scooter, many other parameters such as temperature where not strictly controlled. This result should therefore be compared to complex systems only. As a comparison, a fuel cell bus studied in China showed an voltage decline rate of 346 μ V/h.cell, which is of a similar order of magnitude [29]. In general, degradation rates are found between μ V/h to a few mV/h, depending on the operation of the fuel cell [40]. Our result fit into the

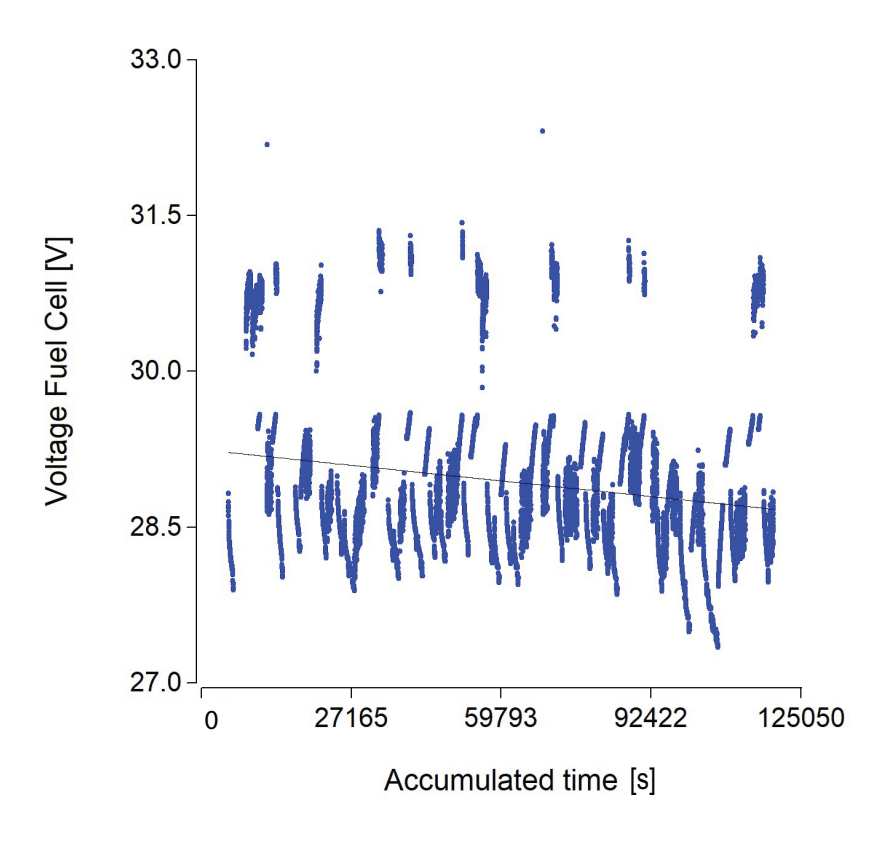


Figure 3.8: Regression model fit for voltage as a function of accumulated time

higher spectrum of this range. The regression relationship derived can only be considered as a rough estimate as a result of the relatively short period of testing of the FCS in this study. Fuel cells used in transportation have an expected lifetime of above 5,000 hours with actual measure lifetimes of about 2,000 hours [41]: 33 hours of testing (including idling time) performed in this study is relatively short.

Figure 3.8 display the regression model in graphical form. The general tendency of the fuel cell voltage in time is downwards. However, variation is also seen which seems more related to the modes. For example, high voltage values above 30 V are a sign of the battery being charged. This happens especially in the V2L mode. It is therefore important to distinguish between modes when performing the degradation rate analysis.

3.5.2. Mode-wise degradation rate

In this section, the degradation rate is calculated per mode.

As previously, a linear fit is used to relate the fuel cell voltage and the operation time. However, we now distinguish each type of mode, yielding three distinct relationships and thus three distinct degradation coefficients. The operation time is the cumulative time per mode in seconds: how many seconds the fuel cell has been performing since the beginning of experiments including idling time.

38 3. Results

Table 3.5: Regression coefficients for fuel cell voltage modelled as a function of cumulative time per mode

	Coef	Est.		S.E.	p-value
		for the entire stack	per cell		
V2L	β0 [V]	30.0	0.75	0.01	<0.0001
	β1 [V/s]	-7.2E-06	-1.8E-07	8.5E-08	0.0406
Drive	β0 [V]	28.8	0.72	2.1E-03	< 0.0001
	β1 [V/s]	-2.3E-06	-5.7E-08	2.9E-08	0.0600
V2G	β0 [V]	28.4	0.71	2.2E-03	< 0.0001
	β1 [V/s]	-4.0E-06	-9.9E-08	3.2E-08	0.0047

The results of the regression model parameters are expressed in table 3.5. Again, all $\beta 1$ slopes are negative and indicate a fuel cell voltage drop for each of the modes. All the model parameter estimates are statistically significant (p<0.05) except for the degradation rate of the driving mode. This is an indication that the usage of the fuel cell in the different modes caused degradation. To increase the significance of the results, more experiments need to be performed. It is likely that the extended usage of the scooter in driving mode would also lead to significant degradation if tested for a longer period of time. In table 3.6, the voltage degradation is translated from V/s to μ V/h.cell. Another way to illustrate these numbers is to calculate for each mode the projected life time, in other words the amount of time the FC can operate when used in this mode only. The end-of-life of a fuel cell is chosen to be the moment the fuel cell voltage has dropped by 10% of its nominal value, which was 24 V [40]. The V2L experiments cause quicker degradation of the fuel cell than the driving or V2G experiments, which translates into a shorter lifetime. The expected lifetime of the fuel cells are above 5,000 hours when using the scooter in the driving mode or the V2G mode. This corresponds to the estimated lifetimes estimated by researchers of the US Department of Energy [41] for FCs used in transportation. V2L usage of the scooter leads to more degradation and thus a smaller lifetime than an average FC vehicle. In fact, least degradation of the FCS was observed when driving the scooter. The scooter was designed for driving, and the Energy Management Strategy (EMS) between the FCS and the battery might have been optimized to guarantee long FCS lifetimes.

Potential decisions that can be taken by the EMS in order to maximize the FC lifetime have been reported to be [42]:

- avoid running at very low currents which could potentially lead to the formation of oxides on the catalyst, thereby reducing its active surface area;
- avoid running at high currents to prevent reactant starvation and excessive temperature which

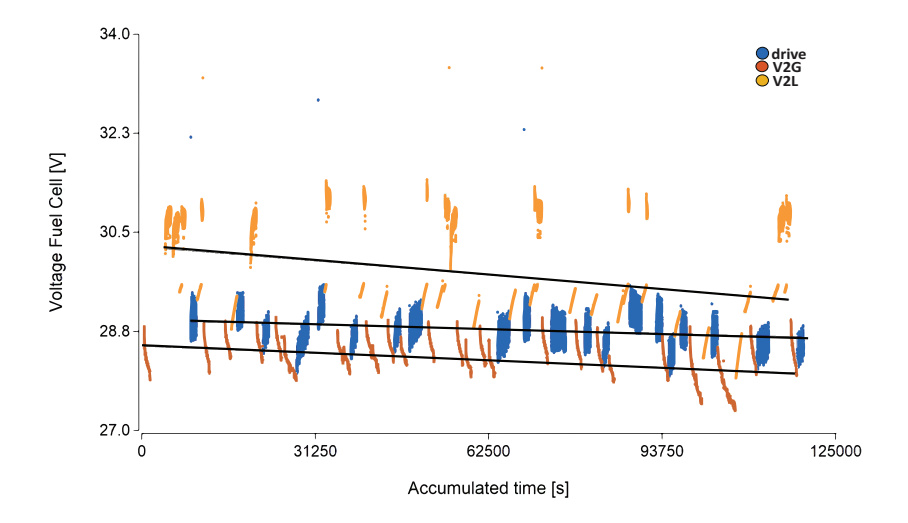


Figure 3.9: Regression model fit for voltage as a function of accumulated time per mode

Table 3.6: Degradation rate and estimated lifetime of an average fuel cell in the fuel cell stack of the scooter for each mode

	Degradation rate [μV/h.cell]	Projected lifetime [h]
V2L	648	3704
Drive	205	11707
V2G	356	6742

would damage the cathode support and dry out the membrane;

- avoid excessive transient loading to maintain stable operating conditions within the fuel cell stack;
- limit start/stop cycles.

In every mode, the scooter was warmed up before use and the fuel cell was never stopped within a run. Therefore, we can discard the effect of the start/stop cycles on the different lifetimes between modes. In the driving mode, the scooter is subjected to varying power demands, or transient loading. However, given the long lifetime calculated from the degradation rate, this transient loading does not seem to cause great damage to the FCS. High currents have a greater effect on the fuel cell degradation rate. The V2G mode is characterized by the fuel cell running at high currents and is enduring a larger voltage drop than the driving mode. Finally, running at very low currents seem to affect the fuel cell the most as V2L usage of the scooter led to the greatest degradation rate of all three modes.

3.6. Voltage drop as a function of current

Figure 3.10 illustrates the polarization curve of the fuel cell stack before and after the 90 experiments performed with the scooter in the three different modes. The voltage of the fuel cell has undergone a

3. Results

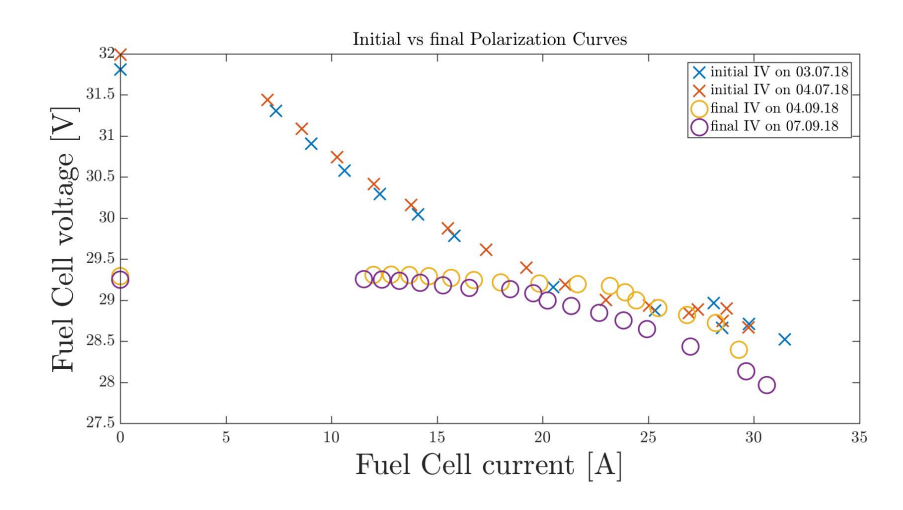


Figure 3.10: Polarization curves of the scooter's FC stack

consequent drop, especially at low current values. From almost 32 V at the start of the experiments, the open circuit voltage of the fuel cell reached 29.2 V at the end of the measurements. Moreover, the range of currents at which the battery kicks in for power supply has increased from 0-7 A to 0-11 A. This is another proof of the degradation of the fuel cells at lower currents, as the battery is now needed to cover those currents in supply. The processes illustrated in figure 3.10 have been quantified per mode, using an empirical model.

A linear regression analysis is chosen to relate the fuel cell voltage with the fuel cell current. This choice is based on the assumption that the irreversibilities encountered by the FC stack occur within the Ohmic region of the polarization curve. Indeed, the fuel cell is mostly operated in the middle range of its operation window, which allows neglecting of the more exponential regions (activation and concentration regions, ref 1.1). Ohmic losses occur due to flow of electrons at cathodes, flow of ions through electrolyte and interconnections between cells and bipolar plates. For each mode, an IV relationship is established between the mean current and mean voltage per event such that:

$$V_{fuelcell} = \beta 0 + \beta 1 * I_{fuelcell}$$
 (3.7)

The results of the regression model are shown in table 3.7 and illustrated in figure 3.11. The slopes of the fitted lines in the figure correspond to the $\beta 1$ coefficients in table 3.7. The lines in the figure are ordered from steepest to least steep: V2L, drive, V2G.

The voltage of the fuel cell decreases upon increasing currents. As shown in table 3.7, all p-values are lower than 0.5, thus the empirical relationships are statistically significant. The slope values $\beta 1$ are a measure for the equivalent resistance of the overall system, given the Ohmic approximation. The steepest degradation line is encountered for the V2L experiments, followed by the drive ones, and finally the V2G experiments. $\beta 1$ is a factor three larger for V2L experiments than for V2G or driving experiments. This indicates the load mode is much more tiresome for the fuel cell. This high

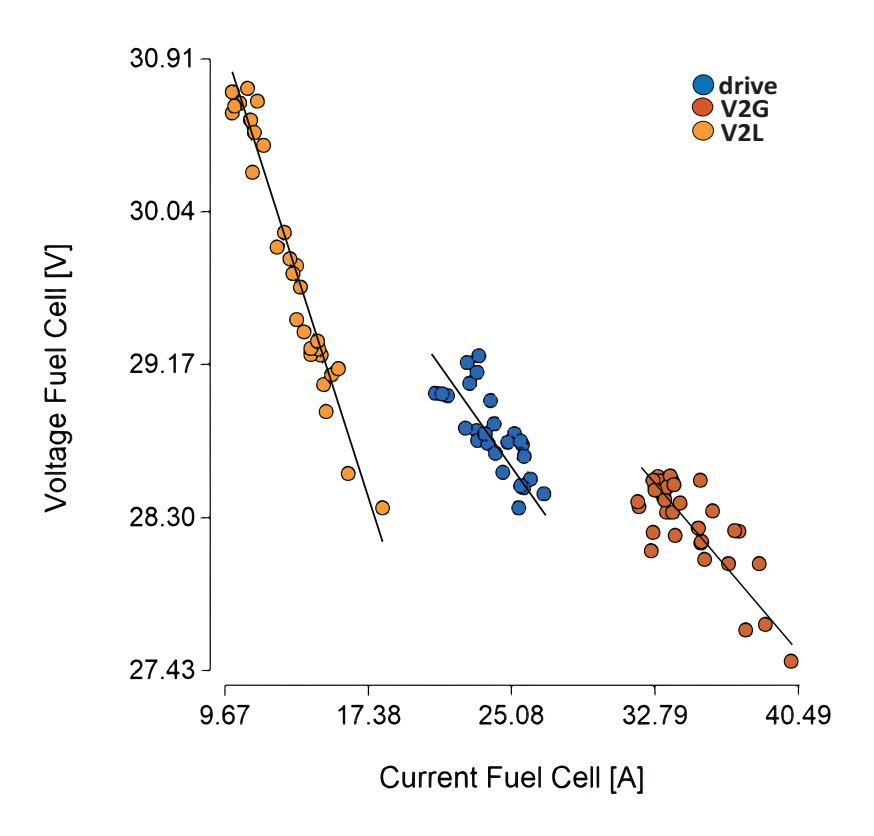


Figure 3.11: Regression lines per mode for voltage fuel cell as a function of current

Table 3.7: Regression coefficients of the IV relationships per mode

	Coef	Est.	S.E.	p-value
D	$\beta 0$	31.57	0.47	<0.0001
	$\beta 1$	-0.12	0.02	<0.0001
G	$\beta 0$	31.59	0.5	<0.0001
	$\beta 1$	-0.10	0.01	<0.0001
L	$\beta 0$	34.08	0.19	<0.0001
	β 1	-0.33	0.01	<0.0001

V2L degradation matches the results found in the previous section, where fuel cell voltage was fitted against time. Resistance increase is an effect of aging. A higher loss of conductivity for the fuel cell can result in a faster degradation of the membrane, corrosion of the plates, dehydration of the membranes or corrosion of the catalyst support.

Interpretation of the results

In this study, a hydrogen fuel cell electric scooter was tested for the first time in view of delivering power for three different applications: to drive, to power the grid (V2G) and to power electric appliances (V2L). In this section, we step back from the technical aspects of this study to dive into the relevance and applicability of the scooter in the future energy system.

4.1. The scooter in the energy system

This study was conducted because of a growing need for flexibility sources in the power system. As intermittent renewable energy sources will take over the power landscape, new energy reserves are sought for to make energy demand and response match. Curtailment can be avoided by dispatching generation storage, using demand-side response, or increase inter-connectivity between the different system components. Meanwhile, making the transition from a fossil to a renewable power supply system comes at a certain investment cost. While the power system should transition to be both sustainable and reliable, final decision making is based on profitability of the system. A way to keep the transition within reasonable cost-limits is to increase the utilization of the power system. The energy system is designed to withstand peak load generation and demand. Shifting the peak load generation to off-peak and flattening the generation curves can be a solution to reduce the expense of the new power system. This eliminates the need for grid expansion by creating a more distributed and connected generation/demand response system.

Electric vehicles have been proven to be a possible tool in producing the flexibility needed in future power systems. The battery or fuel cell system of electric vehicles can be used to store the surplus



Figure 4.1: Energy system of the hydrogen fuel cell scooter: from renewable electricity generation to multi-modal scooter usage

of renewable energy generated. Smart charging strategies can help shifting peak load demand while providing to the vehicle its charging needs for driving. Fuel cell electric vehicles have been proposed as a convenient flexibility provider in the energy system as it does not draw power directly from the grid. FCEV can be operated continuously as long as they have hydrogen supplied. This study on a fuel cell electric scooter fits into this larger picture of providing flexibility to the power system in generating power to capture better the potential of renewable energy generation.

A possible energy system in which the scooter can fit is shown in figure 4.1. This system is mainly characterized by large scale renewable electricity at an optimal production location, transport and storage of the electricity in the form of hydrogen which is filled into canisters at centralized stations before being distributed to retail stored for the end-user (the scooter's driver) to purchase.

At moments when the renewable electricity production surpasses the electricity demand, the surplus of energy needs to be stored. This is done by producing hydrogen from water and electricity using electrolysis. The hydrogen is then stored and shipped to a centralized place. The hydrogen chemical bond in which the hydrogen is stored is an efficient way to dispatch the energy for moments where it is more needed, creating a buffer. The hydrogen gets filled in metal hydride canisters at centralized facilities at a relative low pressure of 10 bars. The cans are then distributed to exchange stations for the consumers to buy them. These exchange stations can be tank stations or retailer stores for example. The rider can purchase new canisters or exchange empty canisters for full ones. Once in possession of the hydrogen canisters, the driver has different possibilities for using its scooter. In the following paragraphs, the applicability of the scooter in each of the modes is discussed.

4.2. Scooter used for driving

The first and principal usage of the scooter is driving, as this is the main motive for a rider to buy such a vehicle. From a usage point of view, the scooter owner expect its vehicle to provide convenient mobility: a pleasant driving experience, a reasonable driving range, ease in handling and refueling.

The scooter used in this study was designed for driving purposes, which means these specifications were taken into account in the conception process. A demonstration project was performed in Taiwan in which 80 scooters similar to the one used in the lab were tested by citizens [43]. The riders reaction about the FCES were positive, showing a first step towards public acceptance of the FCES technology for driving. Besides, fueling of the scooter was experienced as a user-friendly procedure. Changing the canisters takes less than 30 seconds, while the rider does not have direct contact with hydrogen. Moreover, there is no need to bring the vehicle to the place of getting the canister. In this aspect, the FCES is more flexible in usage than a fuel cell electric car for example, where the hydrogen is being fueled as a highly pressurized gas.

From a technical point of view, the scooter's performance in the driving mode was shown to be low in this study. The overall system efficiency of the scooter was evaluated to be 32 % when used for driving. This performance is dependent on the driving cycle performed, which was taken to resemble the Taipei Motorcycle Driving Cycle. The latter is characterized by high acceleration/deceleration and a low average speed. APFCT predicts a range of 60-80 km of driving with two full canisters depending on the driving conditions [44]. Assuming one run of 1024 seconds of TMDC performed in this study is equivalent to 6.8 km, and given an average hydrogen consumption in driving mode of 13.8 g per run, the total distance the scooter can travel on a full tank in TMDC is 44 km. This is well below the driving range announced by the manufacturer. However, this driving range is comparable to the findings of the demonstration tests performed in Taiwan. In the latter case study, the average driving range of the scooters was recorded to be 48.5 km on a full tank [43]. This result is just above the range found in the current study. A driving range of 44-48 km is thus more realistic than 60-80 km. The driving range found in this study is lower than what was found on the road. The difference can be explained by the fact that only one scooter was used in our study, which might have been older and have a slightly lower fuel efficiency than the average scooter. Moreover, the efficiency is very dependent on the driving cycle. In our study, a repetitive driving cycle was applied which was designed to mimic the driving conditions in Taipei. True driving conditions can be very variable and explain the difference in fuel efficiency observed between our lab test and the "on-road" demonstration results.

Nonetheless, the scooter has more applications than merely driving. This study aimed to assess the potential usage of the FCES in both providing mobility and back-up power to the grid and to loads.

4.3. Scooter used in V2G mode

In Vehicle-to-Grid usage, the scooter is used to provide power to the grid in situations where the demand of electricity is higher than the production. The V2G application of the scooter is mainly motivated by grid operators seeking for flexibility sources in their future energy system. As of today,

non-renewable energy production plants are used to provide peak power such as coal and natural gas fired power plants. More intermittent sources would increase the uncertainty in power production and thus increase the need for peaking power plants. Using vehicles as power reserves can reduce the need for new peak power infrastructure. Moreover, allotment of the power and demand sides can alleviate transmission and distribution bottlenecks by providing local reserves.

The feasibility of this overarching goal should be related to the actual potential of the scooter. To give a sense of the impact the scooter can have on the grid, the actual electrical consumption of a Dutch household can be compared with the potential power a scooter can generate in V2G mode. Over a year, the average power consumption of a Dutch household is 3500 kWh electricity [45]. This can be translated to 3500 hours of electricity consumption at a rate of 1 kW, which is the power delivery rate tested in this study for V2G application. This yields an annual hydrogen consumption of 206.7 kg for a Dutch household, or exchanging the two canisters more than 6 times a day on average throughout the day to provide the total needed electricity of the household. In this optic, the scooter as such is not meant for continuous V2G power production. The scooter tested in this study is a vehicle designed for driving purposes to which plug-out features were added. V2G usage was thus not optimized. There is yet no possibility to use the scooter in V2G continuously: the canisters are being emptied simultaneously during the run, which means the scooter turns off when one of the two canisters is removed. A new hydrogen system in which the canisters are being emptied in parallel would enable the renewing of one canister while the other is being used. This is needed for a successful V2G usage.

Taking into account the scale of the scooter, other applications than single household power delivery should be considered. The scooter as a single unit has a limited impact on the grid. However, combining scooters can potentially increase the impact of the vehicles in providing power reserves to the grid. As previous studies focused on parked cars acting as a power plant, scooters could be used in the same perspective [27]. Scooters are currently a popular means of transport for delivery services, such as parcel or food delivery. In times of low delivery activity, scooters stand still on parking lots. A new system could be designed in which these scooters have their capacity bundled to provide power to the grid.

From a technical point of view, the scooter system in this study performs best when used in V2G mode. The overall efficiency of the scooter system is higher than for driving or V2L applications: 39.4 % in V2G against 32.0 and 29.2 % in driving mode and V2L respectively (based on HHV). The higher efficiency of the system is a consequence of the fuel cell stack being operated at almost full capacity, close to 1 kW. This "best performance" of the V2G mode in this study should be related to V2G efficiencies of other systems. A Hyundai fuel cell vehicle was tested in V2G usage at the Green Village providing DC grid power at an efficiency of 45.0 % HHV [19]. In comparison, the scooter is less efficient in converting the hydrogen to grid power. There are multiple plausible reasons for this 5 % lower efficiency of the scooter.

The stage of development of the scooter used in this study is less advanced than for the Hyundai car. The car is already being commercialized which induces a certain level of technological advancement. Though the V2G feature was new in the car's setup too, it can be assumed that the power system as a whole is in a later advancement stage where "learning-by-doing" has helped improving the general system efficiency. The scooter is still at the stage of social and technical demonstration. This implies major improvements can still be made on the technical aspects. For example, the cooling system could benefit further development. As the scooter was run through a V2G event, the temperature rose beyond the the cooling capacity of the water cooling system. Therefore, an additional fan was needed to keep the temperature from reaching 60°C which is the critical temperature the PEM fuel cell stack can endure for proper performance (Appendix E. A better cooling system would be needed thereby improving the overall efficiency. Other elements such as using a load-following blower, or use different topologies of the energy management system could also lead to an improved performance.

4.4. Scooter used in V2L mode

Because of its maximal power capacity of 1.2 kW, the scooter originally appeared to be mostly suited for V2L purposes, providing electricity to appliances behind the grid. In other words, instead of feeding the energy from the scooter to the grid to finally power appliances, the scooter would directly power the appliances within the household. Instead of using electricity which is produced, transported and distributed by grid operators and power producers, and dispatched by an aggregator, using the scooter directly for appliances shortens all the interconnections. The consumer is able to provide for its own consumption with the hydrogen purchased. This can be an efficient way to deviate net congestion, especially at peak hours. When people come home at night, they start cooking, turn on television, charge their appliances. This leads to a high peak of energy demand, which could be covered by V2L usage of personal vehicles. V2L usage benefits mostly the grid operator and the energy provider.

Economic benefits of V2L applications can arise for the consumer as well. When electricity becomes too expensive as a reason of high demand for low real-time production, the consumer can be financially encouraged to use its hydrogen canisters to power its appliances. In this way, new forms of flexibility are created which are both favorable for the infrastructural players and the end-user itself. At this moment, European consumers pay a fixed electricity price of about 21 euro cents per kWh [46]. For an average electrical consumption, this yields a yearly electricity bill of 735€[45]. Considering the average hydrogen usage in V2L mode measured in this study, such a consumption of electricity is equivalent to 311.7 kg hydrogen per year for an average household. In other words, it is economically interesting to power the electrical appliances of a household with the scooter when the hydrogen price falls below 735/311.7 = 2.36€/kg H₂. Hydrogen pricing studies predict future prices at the pump ranging from 2.5

to 6 US\$/kg, which amounts 2.2 to 5.3€/kg [47]. As indicated by the broad range of prediction, future hydrogen prices are hard to forecast and fall beyond the scope of this research. However, a price of 2.36€/kg H₂ would be within the range of predicted prices at the pump. Besides, hydrogen fed at fueling stations might be more expensive than the hydrogen fueled in canisters: hydrogen gas dispensed at a service station is usually pressurized to 700 bars while only 10 bars are needed for canister fueling. In other words, consumers could be motivated to use their scooter to power appliances if electricity prices increases beyond the price of hydrogen. The economic incentive to use hydrogen vehicles as a power source is thought to be the biggest in times of high power demand and low renewable power generation. Further research on the economic part of using FCES for V2X applications needs to be conducted. Nevertheless, the technical reality of V2L usage of the scooter might be a greater barrier for this application to be developed.

Technically, the scooter is limited by its efficiency in V2L usage, with a low system efficiency of 29.2 %. The low power demand in the V2L duty cycle applied to the scooter is thought to be the main cause of this low system efficiency. The duty cycle used in these experiments was designed by combining the signal of one TV, two cell phone and two laptops charging. Combining more loads in order to avoid using the fuel cell at low currents can be a solution to mitigate the low system efficiency found here. However, the loads were originally chosen because of their lack of initial spike in electricity consumption. Most electrical loads of a household contain such an initial peak. This is mostly relevant for resistive load containing a heating element, such as a water cooker or an oven. The scooter used in this study can not be used as such to cover such a peak power demand as its maximum power rate is limited at 1.2 kW. However, new designs could be thought of in which a capacitor is added. This would allow the scooter to provide much higher electrical peaks, and thus cover a broader range of power delivery applications. Transforming the scooter could thus be a potential solution to increase the performance of the scooter in V2L. At this moment, due to its low efficiency and high FCS degradation rate, the scooter is not suited for providing V2L power.

4.5. Degradation of the fuel cell stack

The degradation of the fuel cell stack throughout the 90 experiments performed in this study was 405 μ V/h per cell. This large degradation rate was comparable to the fuel cell stack degradation rate of on-road experiments performed with a FC bus in China [29]. The degradation of a fuel cell stack is a complex issue. Most studies about performance degradation of fuel cells have been conducted on individual fuel cells submitted to controlled accelerated tests. Different degradation mechanisms can be identified, depending on the mode of operation and the type of cell used. However, relating degradation mechanisms to the mode of operation can be difficult as many processes take place which are difficult to measure and interrelated.

To understand the role of the different modes of operation in the fuel cell degradation, separate

degradation rate were calculated for V2L, driving and V2G. As explained in chapter 3, the largest fuel cell degradation rate was found when using the scooter in V2L. In fact, the magnitude of the voltage drop in V2L was 3 times higher than for driving or V2G usage. This leads to the question: what are the characteristics of the V2L duty cycle which might have led to such a severe degradation?

To start with, the load demand in V2L mode was low overall. The average power rate of the fuel cell during a V2L run was 350 W, while it reached up to 1000 W in V2G. Running a fuel cell stack at low currents have been demonstrated to cause degradation [42, 48]. This is confirmed by the polarization curve constructed in 3: the steepest degradation rate is found for V2L operation at low currents. Though the relationship between low current operation and enhanced fuel cell degradation seems well established, there is no consensus on the dominant mechanism causing such degradation. In the next paragraphs, two mechanisms are outlined which have been identified as possible reasons for an enhanced FC stack degradation at low currents.

Enhanced fuel cell stack degradation at low currents can be a result of a disrupted water management in the stack. When operating at low load, the hydrogen gas inlet at the anode is low. As a consequence, the gas pressure inside the stack decreases, which can cause flooding: water is more likely to accumulate, thereby blocking pores meant for gas diffusion. Gas diffusion is needed for the reactants to reach the catalytic surface of the electrode. When flooded, the fuel cell stack voltage drops as well as the fuel cell performance [48]. An excess of water also accelerates corrosion of the electrodes and the catalyst layers. Though water management is pointed out as a critical parameter for fuel cell durability in literature, a clear correlation between current demand and flooding has not been found. In fact, as anode flooding is more likely to occur at low current densities as a result of a lower pressure drop across the cell, flooding can also occur at high current densities because more water is formed at the cathode [49]. Hence, low currents can eventually lead to flooding at the anode but it is not clear whether this is more relevant than flooding of the cathode at higher currents.

Running a fuel cell stack at low current demands can cause the formation of oxides on the catalyst surface which leads to an enhanced fuel cell degradation [42]. Such a mechanism could thus be another reason for the high degradation rate of the fuel cell in V2L mode. Catalyst degradation is mainly a consequence of the harsch conditions found in a FCS. While the anode catalyst is exposed to a strong reducing hydrogen environment, the cathode catalyst has to deal with strong oxidizing conditions. Higher voltages encountered in V2L mode could have resulted in an increase of the electrode potential at the cathode, which is favorable for surface oxides of platinum to be formed. The surface oxides formed decrease the activity of Pt towards the oxygen reducing reaction while leading to an accelerated degradation of the Pt catalyst itself [50].

In fact, many other mechanisms may cause a higher degradation in V2L mode. Water management and Pt degradation are often linked with other processes, such as corrosion or fuel starvation. As

many mechanisms are intrinsically related here, it is difficult to draw conclusions on the exact cause of enhanced degradation in V2L mode.

The V2L mode is also characterized by a varying battery status. Throughout the 30 experiments ran in V2L, the battery was either charging, being by-passed, or charging and then being by-passed. In the first two cases, the power delivered by the fuel cell stack is fairly constant. Avoiding transient loading is known to increase the fuel cell stack's lifetime. Therefore, these cases are not thought to be an additional reason for enhanced FC degradation in V2L. However, an abrupt change in fuel cell power produced is observed whenever the battery stopped charging: no power was needed for the battery anymore and the FC power decreased from about 400 W to 350 W within one second. On average, the FC degradation throughout these V2L with power gradient was higher than for the other V2L cases. From there, it was assumed that the power gradient participated in causing the enhanced degradation rate. However, this should be related to the driving mode. When driving, the fuel cell underwent power gradients that are much larger than in V2L. Therefore, it can be concluded that running the fuel cell at low currents has more impact on the fuel cell degradation rate than applying large power gradients to the system. This conclusion should however be verified by testing fuel cells in the lab under controlled conditions.

5

Discussion

5.1. Remarks on the setup and assumptions

The system design considered in this study has some limitations. It considers the performance of one fuel cell scooter when submitted to different drive cycles. To allow general conclusions on FCES usage in different modes, more scooters need to be tested. The results from this study should be interpreted as a first demonstration testing.

The duty cycles designed for this study have been adapted to the electronic load available for the experiments. As a consequence, peaks of power demand above 1 kW were truncated which prevented a thorough analysis of the system at maximal capacity. Another electronic load could be used in further studies.

In view of the time constraints of this study, it was chosen to perform 90 experiments in total. As a result, degradation processes occurring in a specific age frame of the FCS might have been highlighted, while other degradation processes might have been overlooked. For a complete degradation analysis of the fuel cell system, more runs need to be performed. This will help improving the accuracy of the estimated fuel cell stack lifetime.

In this study, system efficiencies were calculated for each mode. These efficiencies depend greatly on the average mass of hydrogen consumed per mode. Because of erroneous sensor measurements, it was chosen to estimate the mass of hydrogen consumed by weighing the canisters before and after events and correct for the idling time C. Though this method was estimated to yield the most accurate results, it is still prone to uncertainties. The weighing scale used in the lab had a resolution of 0.1 g, which is the measure of the smallest detectable increment. However, repeatedly measuring the same canister has yielded results within a range of 0.5 g. The canister mass measurements performed

5. Discussion

with this scale have thus a precision of \pm 0.25 g. Such a deviation in mass measurement leads to an uncertainty of up to \pm 1% for the V2L mode. In future work with the scooter, the hydrogen mass consumed throughout the tests should be monitored more accurately. Either the sensor should be replaced, or the weighing of the canisters should be done more consistently throughout the study.

When modelling fuel cell degradation, the fuel cell stack voltage and current were assumed to be linearly related. In other words, the linear ohmic losses were assumed to be more important in the studied window of currents than the logarithmic activation losses. The resulting linear IV relationships per mode were statistically significant. However, most of the fuel cell stack degradation is seen at relative low currents. In literature, activation losses are found to be most important at "low currents" as well [11]. This would compromise the linear assumption made here. Nonetheless, "low" is a relative concept, which should be related to cell size and number. To verify the appropriateness of the ohmic assumption, current values should be converted to current density (mA/cm²) for a fair comparison with literature values. However, the area of the cells was not known in this study. Therefore, the ohmic losses were estimated larger than the activation losses, leading to a linearity assumption.

5.2. Recommendations for future work

Throughout this work, several of directions of research have been identified which were considered out of the scope of this study. Further research could include these aspects for a better understanding of the scooter fuel cell system.

On a **system level**, research is encouraged regarding the following points:

- Aggregate scooters in a parking lot for combined power delivery to the grid
- Assess the environmental impact of using fuel cell scooters in combined modes: how does powering homes via V2G or V2L help reducing GHG emissions? This would include research on hydrogen fuel production pathways.
- Assess the profitability of using a scooter in combined modes for both the consumer and the grid operator.

On a **fuel cell stack level**, further investigation in the following topics is encouraged:

- Explain further the role of the battery state in the higher degradation rate found for the V2L mode. This could be done by controlling the battery state in a decoupled system.
- Assess the exact energy management strategy of the scooter and how it affects the fuel cell system's working.
- Quantify the effect of pressure gradients on fuel cell degradation independently of the battery's state.

6

Conclusion

In a context of global urbanization and increasing personal mobility, scooters have been taking over urban landscapes. However, the increased number of vehicles on the roads are causing both a threat to the environment and local air quality. Electric vehicle have been proposed as a solution to mitigate carbonated emissions and provide a clean way of transport when electricity is produced from renewable resources. Fuel cell electric vehicles are mostly interesting regarding their fast refueling time and extended driving ranges. Hydrogen is considered as a promising fuel as well as energy carrier. In the future, surplus electricity could be transformed into hydrogen through electrolysis for ulterior usage: conversion to hydrogen creates buffers of energy storage. Flexibility can also be created using electric vehicles as power sources. Using the electric vehicle fleet to power the grid or power appliances directly is a way of creating frequency reserves as well as alleviating possible grid congestion. However, the development of fuel cell vehicles has been hindered by the performance of their fuel cell, which is dependent on its usage. This led us to formulating the main research question:

How does the combined use of a hydrogen fuel cell scooter for driving, V2L and V2G purposes affect its performance?

To answer this question, a scooter was experimentally used to provide energy to drive, power an electrical appliance (V2L) and power the grid (V2G). Duty cycles were designed to mimic usage in each mode. The duty cycles were applied to the scooter via a programmable electronic load. The experiments were performed 30 times per mode.

An exploratory analysis of the data collected throughout the experiments was used to answer the first subquestion: **How does the scooter perform in each mode?** To evaluate the scooter's performance, the different energy management strategies were compared. The scooter has two power

54 6. Conclusion

sources, a hydrogen fuel cell and a battery. The power provided by the vehicle as a whole is a combination of the power produced by each of these components at a certain time step. As the power demand differed in each mode, different energy management strategies between the fuel cell and the battery were observed. In the V2G mode, a high and constant power had to be delivered. The fuel cell took up the largest part of the energy share, being backed-up by the battery at the start when the fuel cell was not warm enough. In driving mode, the power demand was characterized by large and abrupt fluctuations. This was reflected by quickly changing power shares of the fuel cell and the battery. In V2L mode, the power demand was low. The fuel cell could produce the necessary power even at low temperatures while the battery was either being charged or by-passed. The system efficiency was calculated to quantitatively assess the performance of the scooter is each mode. V2G usage of the scooter resulted in the highest efficiency (39.4% based on HHV) as the fuel cell operated at almost full load. V2L was the least efficient mode (29.2%).

A principal component analysis (PCA) was used to identify the variables leading to discriminating the three modes of operation. The variability between the modes could mainly be explained by the fuel cell and battery voltage.

To answer the second subquestion: **How does the fuel cell degrade in each mode?**, a set of linear regression analyses were performed. An overall degradation rate of 405 μ V/h per cell was measured. Such a high decay rate is comparable to on-road study performed with a fuel cell bus in China. The third subquestion **Which mode leads to more degradation of the fuel cell?** was answered by segregating the decay rates per mode. This yielded a higher voltage drop of 648 μ V/h in V2L mode, which is a consequence of the low operating power and high operating voltage of the fuel cell in this mode. Constructing an IV curve for the fuel cell stack confirmed this finding: operating the fuel cell at low currents in V2L mode has led to the largest voltage drop. Possible reasons for a higher degradation at low current operation can be an increased flooding of the stack, or reduction of the active surface area of the catalyst. The testing time of the scooter's fuel cell system can be increased to improve the statistical significance of the degradation rates and unravel the exact mechanisms behind the increased degradation in V2L.

From this study, it can be concluded that the scooter should not be used as such for combined V2L, V2G and driving. The actual energy management system has been conceived to minimize fuel cell degradation in driving mode. A new specific energy management system for V2L and V2G operation could be designed for parallel operation to driving. The focus should be laid on high operating power and high fuel cell current operation to minimize the fuel cell voltage decay and increase the overall system performance.

- [1] M. Hanlon, *The scooter- a short history of a cultural icon*, Website. https://newatlas.com/go/3954/ (2015), accessed on 23.10.2018.
- [2] F. Kamakate and D. Gordon, *Managing motorcycles: Opportunities to reduce pollution and fuel use from two-and-three wheeled vehicle,* International Council on Clean Transportation (ICCT) (2009).
- [3] S. Platt, I. E. Haddad, S. Pieber, R.-J. Huang, A. Zardini, M. Clairotte, R. Suarez-Bertoa, P. Barmet, L. Pfaffenberger, R. Wolf, et al., Two-stroke scooters are a dominant source of air pollution in many cities, Nature communications 5, 3749 (2014).
- [4] United Nations (UN), *Adoption of the paris agreement,* Framework convention on climate change (2015).
- [5] IPCC, Contribution of working group iii to the fifth assessment report of the international panel on climate change, Mitigation of climate change (2014).
- [6] International Energy Agency (IEA), *Towards sustainable urban energy systems,* Energy technology perspectives 2016 (2016).
- [7] D. Kolokotsa, *The role of smart grids in the building sector*, Energy and Buildings **116**, 703 (2016).
- [8] R. Sims, R. Schaeffer, F. Creutzig, X. Cruz-Núñez, M. D'agosto, D. Dimitriu, M. Figueroa Meza, L. Fulton, S. Kobayashi, O. Lah, et al., Chapter 8: transport, Climate Change 2014: Mitigation of Climate Change. Contribution of Working Group III to the Fifth Assessment Report of the Intergovernmental Panel on Climate Change (2014).
- [9] J. J. Hwang, Sustainable transport strategy for promoting zero-emission electric scooters in taiwan, Renewable and Sustainable Energy Reviews **14**, 1390 (2010).
- [10] A. van Wijk, The Green Hydrogen Economy in the Northern Netherlands, Tech. Rep. (Noordelijke Innovation Board, 2017).
- [11] J. Larminie, A. Dicks, and M. S. McDonald, *Fuel cell systems explained*, Vol. 2 (J. Wiley Chichester, UK, 2003).
- [12] A. Van Wijk and L. Verhoef, *Our car as power plant* (Ios Press, 2014).

[13] B. Mathiesen, H. Lund, D. Connolly, H. Wenzel, P. Østergaard, B. Möller, S. Nielsen, I. Ridjan, P. Karnøe, K. Sperling, and F. Hvelplund, Smart energy systems for coherent 100% renewable energy and transport solutions, Applied Energy 145, 139 (2015).

- [14] W. Kempton and S. E. Letendre, *Electric vehicles as a new power source for electric utilities,* Transportation research. Part D, Transport and environment **2**, 157 (1997).
- million electric vehi-[15] E360 Digest, Europe now has one the cles on road, Website. https://e360.yale.edu/digest/ europe-now-has-one-million-electric-vehicles-on-the-road (2018), accessed on 24.10.2018.
- [16] Eurostat, Maximum electrical capacity mw eu-28, Website. https://ec.europa.eu/eurostat/statistics-explained/index.php?title=File:Maximum_electrical_capacity, MW, EU-28, 2000-2016.png (2016), accessed on 24.10.2018.
- [17] European Automobile Manufacturers Association, *Vehicles in use europe 2017*, Website. https://www.acea.be/statistics/article/vehicles-in-use-europe-2017 (2017), accessed on 24.10.2018.
- [18] P. Ahmadi and E. Kjeang, *Realistic simulation of fuel economy and life cycle metrics for hydrogen fuel cell vehicles,* International Journal of Energy Research **41**, 714 (2017).
- [19] Hyundai, *Hyundai nexo*, Website. https://www.hyundaiusa.com/nexo/index.aspx, accessed on 14.09.2018.
- [20] Toyota, *Toyota mirai*, Webiste. https://www.toyota.nl/modellen/mirai/index, accessed on 14.09.2018.
- [21] Honda, Honda clarity series- electrified vehicles, Website. https://automobiles.honda.com/clarity, accessed on 14.09.2018.
- [22] C. Tso, L.-H. Huang, and C.-J. Tseng, *Hydrogen scooter testing and verification program,* Energy Procedia **29**, 633 (2012).
- [23] E. Wiseman, Metropolitan police trial hydrogen fuel cell scooter, Website. https://www.telegraph.co.uk/cars/news/metropolitan-police-service-trial-hydrogen-fuel-cell-s (2017), accessed on 28.10.2018.
- [24] B. Purvis, Hydrogen fuel cells: is it the future for motorbikes? Website. https://www.bennetts.co.uk/bikesocial/news-and-views/features/bikes/hydrogen_powered_bikes_future_fuel (2017), accessed on 28.10.2018.

[25] METI, Compilation of the revised version of the strategic roadmap for hydrogen and fuel cells, Website. http://www.meti.go.jp/english/press/2016/0322_05.html, accessed on 17.09.2018.

- [26] CEP, Clean energy partnership, Website. https://cleanenergypartnership.de/en/home, accessed on 17.09.2018.
- [27] M. Poorte, Technical and economic feasibility assessment of a Car Park as Power Plant offering frequency reserves (TU Delft repository, 2017).
- [28] C. B. Robledo, V. Oldenbroek, F. Abbruzzese, and A. J. van Wijk, *Integrating a hydrogen fuel cell electric vehicle with vehicle-to-grid technology, photovoltaic power and a residential building,* Applied Energy **215**, 615 (2018).
- [29] J. Li, Z. Hu, L. Xu, M. Ouyang, C. Fang, J. Hu, S. Cheng, H. Po, W. Zhang, and H. Jiang, *Fuel cell system degradation analysis of a chinese plug-in hybrid fuel cell city bus,* international journal of hydrogen energy **41**, 15295 (2016).
- [30] K. Jennifer, S. Sam, A. Chris, and S. Genevieve, *Fuel cell Electric Vehicle Evaluation*, Tech. Rep. (National Renewable Energy Lab.(NREL), United States, 2015).
- [31] V. Oldenbroek, L. A. Verhoef, and A. J. van Wijk, Fuel cell electric vehicle as a power plant: Fully renewable integrated transport and energy system design and analysis for smart city areas, International Journal of Hydrogen Energy **42**, 8166 (2017).
- [32] Kikusui Electronics Corp., Users' manual: Electronic load plz-4w series, (2015), version 2.
- [33] B. Lin, *Conceptual design and modeling of a fuel cell scooter for urban asia,* Journal of Power Sources **86**, 202 (2000).
- [34] R. Maceiras, V. Alfonsin, A. Cancela, and A. Sanchez, *Modellization of metal hydride canister for hydrogen storage*, European Journal of Sustainable Development **4**, 129 (2015).
- [35] K.-h. Young and J. Nei, *The current status of hydrogen storage alloy development for electro-chemical applications,* Materials **6**, 4574 (2013).
- [36] L. Lu, X. Han, J. Li, J. Hua, and M. Ouyang, *A review on the key issues for lithium-ion battery management in electric vehicles,* Journal of Power Sources **226**, 272 (2013).
- [37] G.-H. Tzeng and J.-J. Chen, *Developing a taipei motorcycle driving cycle for emissions and fuel economy,* Transportation Research Part D: Transport and Environment **3**, 19 (1998).
- [38] S. Barker, S. Kalra, D. Irwin, and P. Shenoy, *Empirical characterization and modeling of electrical loads in smart homes*, in *Green Computing Conference (IGCC)* (IEEE, 2013) pp. 1–10.

[39] L. Placca, R. Kouta, D. Candusso, J.-F. Blachot, and W. Charon, *Analysis of pem fuel cell experimental data using principal component analysis and multi linear regression,* International Journal of Hydrogen Energy **35**, 4582 (2010).

- [40] J. Wu, X. Z. Yuan, J. J. Martin, H. Wang, J. Zhang, J. Shen, S. Wu, and W. Merida, *A review of pem fuel cell durability: Degradation mechanisms and mitigation strategies,* Journal of Power Sources **184**, 104 (2008).
- [41] DOE, US Department of Energy, Targets for polymer electrolyte membrane fuel cell components, Website. https://www.energy.gov/eere/fuelcells/doe-technical-targets-polymer-electrolyte-membrane-fuel-cell-components ((n.d.)).
- [42] T. Fletcher, R. Thring, and M. Watkinson, *An energy management strategy to concurrently optimise fuel consumption & pem fuel cell lifetime in a hybrid vehicle,* international journal of hydrogen energy **41**, 21503 (2016).
- [43] Breakthrough Technologies Institute, *Taiwan hydrogen fuel cell scooter fleet demonstration,* Information obtained via APFCT (2013).
- [44] J. J. Hwang, *Review on development and demonstration of hydrogen fuel cell scooters,* Renewable and Sustainable Energy Reviews **16**, 3803 (2012).
- [45] Energiesite, Wat is een gemiddeld energieverbruik? Website. https://www.energiesite.nl/veelgestelde-vragen/wat-is-een-gemiddeld-energieverbruik/, accessed on 10.11.2018.
- [46] Eurostat, Electricity prices for household consumers, Website. https://ec.europa.eu/eurostat/statistics-explained/index.php/Electricity_price_statistics# Electricity_prices_for_household_consumers, accessed on 7.11.2018.
- [47] International Renewable Energy Agency, *Hydrogen from renewable power: Technology outlook* for the energy transition, Tech. Rep. (2018).
- [48] X. Hu, K. Song, N. Wenxu, and T. Zhang, *Powertrain System Durability in Proton Exchange Membrane Fuel Cell Electric Vehicles: A Review*, Tech. Rep. (SAE Technical Paper, 2018).
- [49] W. Schmittinger and A. Vahidi, *A review of the main parameters influencing long-term performance and durability of pem fuel cells,* Journal of Power Sources **180**, 1 (2008).
- [50] Y. Shao, G. Yin, and Y. Gao, *Understanding and approaches for the durability issues of pt-based catalysts for pem fuel cell*, Journal of Power Sources **171**, 558 (2007).
- [51] J. Yin, Y. Shen, X. Liu, G. Zeng, and D. Liu, Research on state-of-charge (soc) estimation using current integration based on temperature compensation, IOP Conference Series: Earth and Environmental Science, **94**, 012165 (2017).



TMDC: from velocity to instantaneous power demand

A.1. Model structure

The instantaneous power demand is derived from the forces acting on the scooter. These are illustrated in figure A.1.

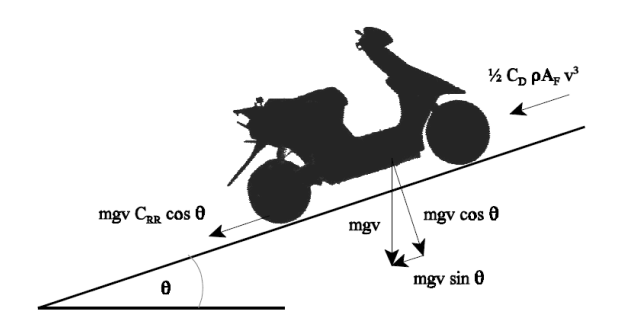


Figure A.1: Free-body diagram of the scooter [33]

$$P_{wheels} = (mav) + (mgvsin\theta) + (mgvC_{rr}cos\theta) + (1/2\rho_{air}C_DA_fv^3)$$
(A.1)

Each term in between brackets of equation A.1 represents respectively: acceleration, slope, rolling resistance and aerodynamic drag.

The variables are:

- m=total mass of the vehicle, including passenger
- θ =angle of the slope
- a=acceleration of the vehicle
- v=velocity of the vehicle
- C_{rr}=coefficient of rolling resistance
- ρ_{air} =density of the air
- *C*_D=drag coefficient
- A_f=frontal area

Besides the power needed at the wheels, extra power is needed to cover up for inefficiencies. The total power needed is a sum of the power needed at the wheels, the power needed for auxiliary functions such as the headlights or the dashboard and the parasitic power needed for the proper functioning of the fuel cell.

$$P_{needed} = P_{wheels} / \eta_{drivetrain} + P_{aux} + P_{parasit}$$
 (A.2)

A.2. Model parameters

In order to use the model, certain parameters need to be known. It has been chosen to work mostly with the parameters a estimated in [33]. These are actually based on known data from electric scooters. The mass of the vehicle is the one given by APFCT, 105 kg, on which a 75 kg person is added. Also, the 77% drivetrain efficiency comprises the efficiency of the motor, the booster, the gear-chain and the transmission losses. A constant value of 100 W is taken for the parasitic losses. These losses are typically losses linked to the use of fans and pumps for the system to cool down and to evacuate the unnecessary components. Taking a constant value is an approximation, as in reality, these losses scale with the power output.

Using this model, the power needed is derived and can be viewed in figure A.2.

Table A.1: Model parameters for TMDC

Parameter	Value
m (kg)	105+75
C_{rr}	0.014
C_d	0.9
A_f	0.6
$\eta_{drivetrain}$	0.77
$ ho_{air}$	1.23
P_{aux} (W)	60
P_{para} (W)	100

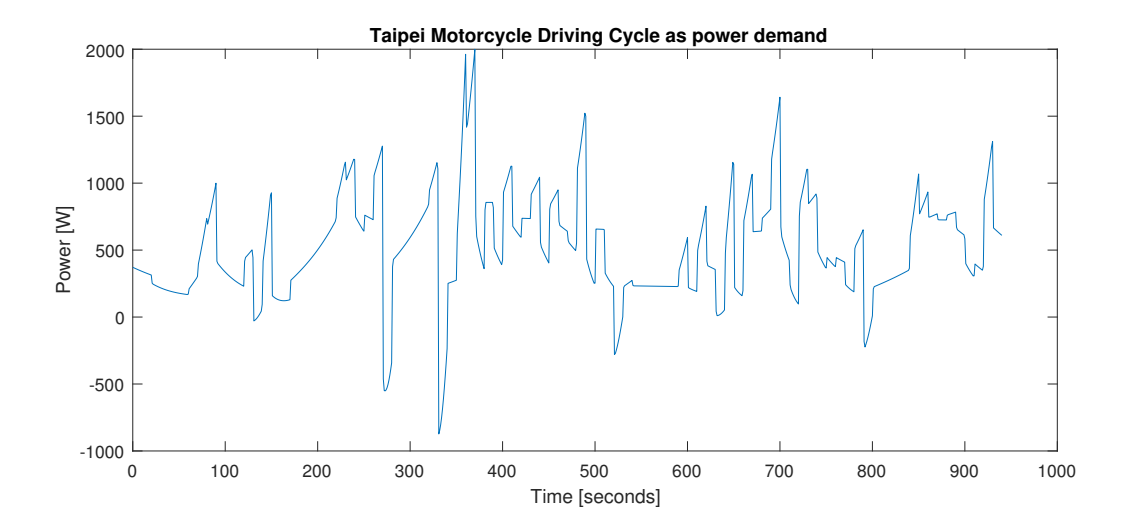


Figure A.2: TMDC in power units, as converted by the physical model

B

List of experiments

			nτ	Date	Hour	Expe	erime	nt Date	Hour
1	2G	1	*	6 july 18	9h40.	29D	49	14 aug 18	
2	8D	v		Gjuly 18	13h 28	20D	48	14 aug 15	11h 09
3	23L		1	10 july 18	11 h 45	29L	49	14 aug 18	
4	24L			10 july 18	13 h 51	7D	50	1	15h05
S	1L			10 july 18	15h59	5L	21	39970	
6	1D			16 3111118	9122	4L	57		13 46
7	19L			16 74/4/8	11 1022	23G	5	10000	15h52
8	25G			16 july 18	13443	13D	25	100	17h 12
a	28D			16 july 18	16 h 10	_	85	1/	& h50
10	21D	top	8	81 WW F1	9416	26D	26	The standing	10 h37
	6G	,	1	17 14118	il n 05	30L	23	- AUGUAN	12 h54
12	14L		\top	12 july 18	13 610	18G		10 000	14 h 46.
13	30D		\top	17 july 18			28		16h30.
	9L		+		15h15	-	59	17 aug 18	9404
	27G		+	1 210 10	9h23	18L	60	Sipup 1	11 h22
	5D		+	July	10h54	17G	61	17 aug 18	13/109
-	15L		+	July 10	12 434	15D	62	A avg 18	14h58
, –	15G		+	18 july 18	14 h 32.	21G	63	17 angle	17h 08
-	19G	,	+	18 july 18	16411	28L	64	27 040 18	9000
, ,	14G		+	19 July 18	9425	26L	65	27-08-18	10h34
	24D		+	19 july 18	11 h54	17D	66	27-08-18	12,405
_	LOD		+	19 july 18	13h 38	18D	67	27-08-18	13 h 56
23 1			╀	19 july 18	15h 18	27L	68	27-08-18	16419
			\vdash	Shigefor	13/31	19D	69	28 - 08 -18	FIRE
_	.5L			20 july 18	15/104	3G	70	28 - 08 -18	11 622
	2G	•	-	23-01-18	14/104	3D	71	28-08-18	13 h34
_	8G	(23-07-18	15h58	10L	72	28 - 08 - 18	15 h43
	2D		_	23-07-18	18h12	11D	73	28-08-18	17 405
	0L			24-07-18	9403	9G	74	29-08-18	8 h13
'	00		1	24-02-18	10 h37	4G	75	29-08-18	10h12
-	9G	ł.		24-07-18	12h50	22L	76	29-08-18	15 h26
_	2L			25-07-18	9405	25D	77	30-08-18	9h05
2 80			-	25-07-18	10 1, 46	20G	78	30-08-18	10h35
3 16				25-07-18	12 h 59	5G	79	30-08-18	12h304.
1 13	3G		-	B1-FO-25	15 h 28	16G	80	30-08-18	
5 12	2D		2	81-50-2	10 h 58	7L	81	30-08-18	14h31
90)		9		12443	2L	82	20 00 10	
6L			2	0	15h03	11G	83	31-08-18	9h58
8 22	G.	4	21	2-07-18	17h05	23D	84	31-08-18	11 h29
21	L		2	81-50-5	9 h 5 8	4D	85		13 h 33
8L			2	1	11h 28	16L	86		15h28
11	L		2	1	13h44	3L	87	3-09-18	9h24
, 7G	i		3	7-07-18	15 h33.	17L	88	3-09-18	10 / 51
240	G		30	1-07-18	12 M35.	1G		3-09-18	12424
131		_	30	10		27D	89	3-09-18	13h 57
300			بر. 30		15404	2/0	90	3-09-18	15h56
	-	1	Y	-03-18	16h44		- 1		

Figure B.1: Order and time of experiments



Calibration curves

Measurements were performed throughout the experiments using sensors which were installed in the scooter beforehand. While the temperature sensors was gauged to provide directly the temperature in °C, the other sensors had to be calibrated in order to get the signal in an appropriate unit for further analysis. In this appendix, the different calculations done to convert the originally measured signal to a usable one are highlighted.

C.1. Pressure calibration

The pressure is measured by means of a Texas Instruments pressure sensor (Nr 68CP042) To convert the pressure signal received in volt at the data logger to a signal in bar, the following formula was used:

$$P_{vsi} = P_{volt} - 0.513) * 75 (C.1)$$

$$P_{bar} = P_{psi} * 0.0689475729 \tag{C.2}$$

This formula was provided as such by APFCT.

C.2. Current calibration

The current is measured at three different points in the electric circuit of the scooter: measurements were performed in-line after the FC, after the battery and before the output connector. The sensors used are from series L01ZxxxS05, manufactured by Tamura Corporation.

Conversion formula's were provided by APFCT but appeared to yield erroneous results. Therefore it was chosen to calibrate again the current signals using constant current tests. These tests were performed before the start of the experiments. A set current was applied to the electronic load, while

66 C. Calibration curves

the current signal in volts was gathered by the data logger and the real current in amps was measured using a current probe which was clamped around the wire going out of the FC, battery and booster respectively.

$$IFC_A = (-IFC_V - 2.5986) * 68.148$$
 (C.3)

$$Ibatt_A = (Ibatt_V - 2.583941) * 90.54$$
 (C.4)

$$Iout_A = (Iout_V - 2.61784) * 72.961$$
 (C.5)

C.3. Hydrogen mass calibration

The mass of hydrogen present in the canisters at a given moment is measured as a voltage signal between 5 to 1 V. As soon as the canisters are filled and clicked in the scooter, a gauge button is pressed in to make the signal start at 5 V: the maximum mass available which is the sum of hydrogen present in the two canisters. This is the amount of hydrogen fuelled, which can be maximum 90 grams.

In order to calibrate the voltage signal to a mass signal, several methods were carried out and will be explained here. Each of the methods present disadvantages which will be outlined.

Getting the hydrogen content of the canisters is necessary in order to know the hydrogen consumption per experiment: this is then used for efficiency calculations.

C.3.1. Linear fit from voltage signal

In order to know the hydrogen content of the canisters present in the scooter at all times during an experiment, a linear relation was sought between the voltage signal received by the data-logger and the true mass of hydrogen contained in the canisters.

To establish the relationship between voltage and mass, we measured the mass of the canisters before each experiments. This was done using a scale of precision xxx. The mass of the hydrogen contained was then deduced by subtracting the empty canister mass from the measured mass. This mass was related to the voltage signal measured by the sensor at the start of an experiment.

Fitting the mass of hydrogen and the voltage signal measured yields the linear relationship displayed in figure C.1.

The high r-square indicates a robust linear fit. However, using this relationship for further calculations has highlighted its main default: the relationship is extremely sensitive to the fit applied. If the fit is slightly different, taking for example one point less, the mass consumption per experiment changes up to 3 grams. This influences the results too much, which led to discarding this method. It has been decided not to work with the voltage signal further, as it is considered to be a too big source of inaccuracies.

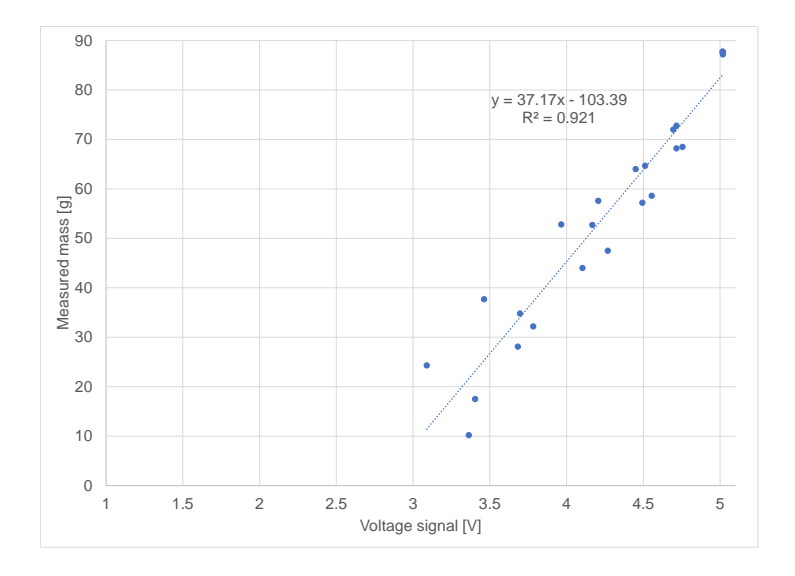


Figure C.1: Calibration curve of the hydrogen mass contained in the canisters

C.3.2. Corrected Faraday consumption

Now the voltage signal is discarded as a way to measure the mass of hydrogen consumed throughout the experiments, we can turn to the theoretical amount of hydrogen consumed inside the fuel cell stack.

Faraday's law defines the molar flow of reactant consumption as follows:

$$n_{H_2}^{\cdot} = \frac{I_{stack}.N_{cells}}{2.F} \tag{C.6}$$

I is the stack current, N the amount of cells (40), 2 is the amount of exchanged electrons per mole of hydrogen and F is the Faraday constant. Multiplying by the molar mass of hydrogen (2 g/mole) yields the following relationship:

$$m_{H_2} = \frac{I_{stack}.N_{cells}}{F} \tag{C.7}$$

In order to visualize how Faraday's law estimates the amount of hydrogen consumed in an event, a plot was made displaying the measured mass consumed in an event against the calculated mass from Faraday's law. From figure C.2, it appears that Faraday's law underestimates systematically 1.35 g hydrogen consumption per experiment. However, the rate of consumption seems well described by the relationship.

C.3.3. Measured masses with idling time correction

In order to calculate the efficiency of the scooter per mode, the average consumption of hydrogen per mode must be known. From the mass measurements made, we know the average hydrogen

68 C. Calibration curves

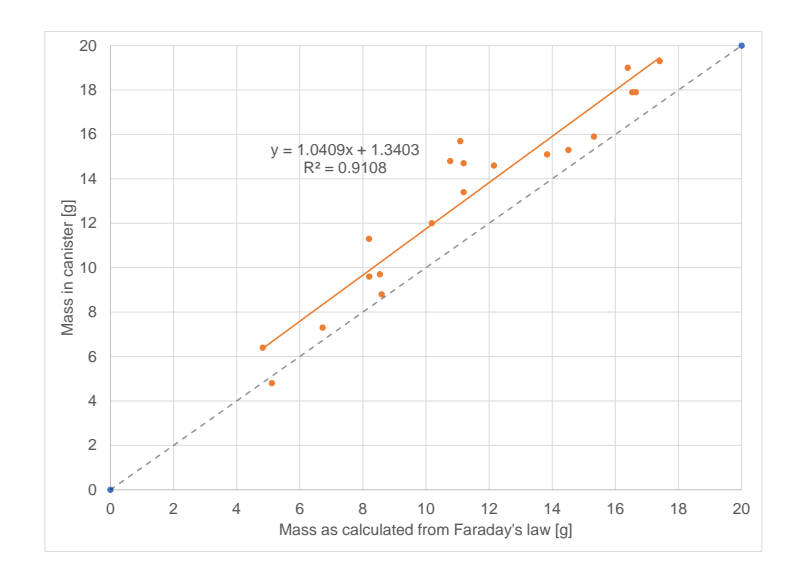


Figure C.2: Real mass of hydrogen against estimates from Faraday's law

consumption of a complete experiment, which includes idling time. In this part, we estimate the average hydrogen consumption per event without idling time.

In order to correct for the idling time, an additional experiment was performed where the scooter was put to idle for 2 hours. The mass of the canisters was measured before and after the experiment, which yields a total hydrogen consumption of 19.6 g, or 2.72 mg/min. The temperature of the scooter increased throughout the experiment from 24.6 to 39.2 °C, which is assumed to be a representative range of operation the scooter was in throughout the tests including idling we want to correct.

Per test for which the mass is known and the idling is included, we correct the hydrogen by subtracting the amount of hydrogen consumed during the idling time.

This method can be disputed considering the amount of hydrogen consumed in the idling time. The starting up of the scooter probably takes more hydrogen than the rest of the time, making the consumption per minute somewhat biased.

C.3.4. Summary

Each of the methods previously stated yields a different average hydrogen consumption per mode. Then results are summarized in table C.1. The linear fit from the voltage signal yields values that are highly underestimating reality. The Faraday equation helps understanding what is at least needed by the fuel cell to produce a certain amount of energy. The measured mass without correction for the idling time overestimate the consumed hydrogen. We therefore chose to work with the corrected values.

Table C.1: Average hydrogen consumption per mode in gram

	Linear fit	Linear fit from	Measured mass	Measured mass
	from voltage signal	Faraday equation	w/o idling correction	w/idling correction
Drive	9.9	11.9	14.2	13.8
Grid	11.12	16.6	17.2	16.8
Load	5.29	7.2	8.6	7.6



Energy management strategy in V2L experiments

Vehicle-to-Load experiments showed different energy management strategies (EMS): the share of power production between the fuel cell and the battery varied from run to run. Three categories of different EMS were identified: 1. the battery was being charged throughout the whole run, 2. the battery was being by-passed throughout the whole run and 3. the battery was first being charged and then by-passed. The EMS of each V2L experiment is depicted in figure D.1. Table D.1 gives a classification of the runs per category. In 11 of the 30 experiments, the battery was constantly charging, in 8 cases it was by-passed, and in the remaining 11 cases, the battery was first charged then by-passed.

A reason for this alternating behaviour of the battery between the runs of V2L experiments can be found in the State-of-Charge (SOC) of the battery itself. When the battery is full, there is no need for further charging and the battery can be by-passed. To verify this, the points at which the battery stopped being charged to be by-passed were identified. The SOC of the battery was derived in time, throughout all the experiments. This was done using the formula:

$$SOC(t) = SOC(t-1) - \frac{I_{batt}(t)}{3600 * C_{batt}}$$
(D.1)

where the initial SOC estimated at 50%, and the battery capacity was known to be 20 Ah. The capacity represents the amount of charge that the battery can deliver at rated voltage (24 V), and is proportional to the amount of electrode material contained in the battery.

In figure D.2, the SOC is plotted in time. Red dots indicate the moments at which a change in battery behavior was noticed in the V2L experiments, with the corresponding SOC of the battery. The

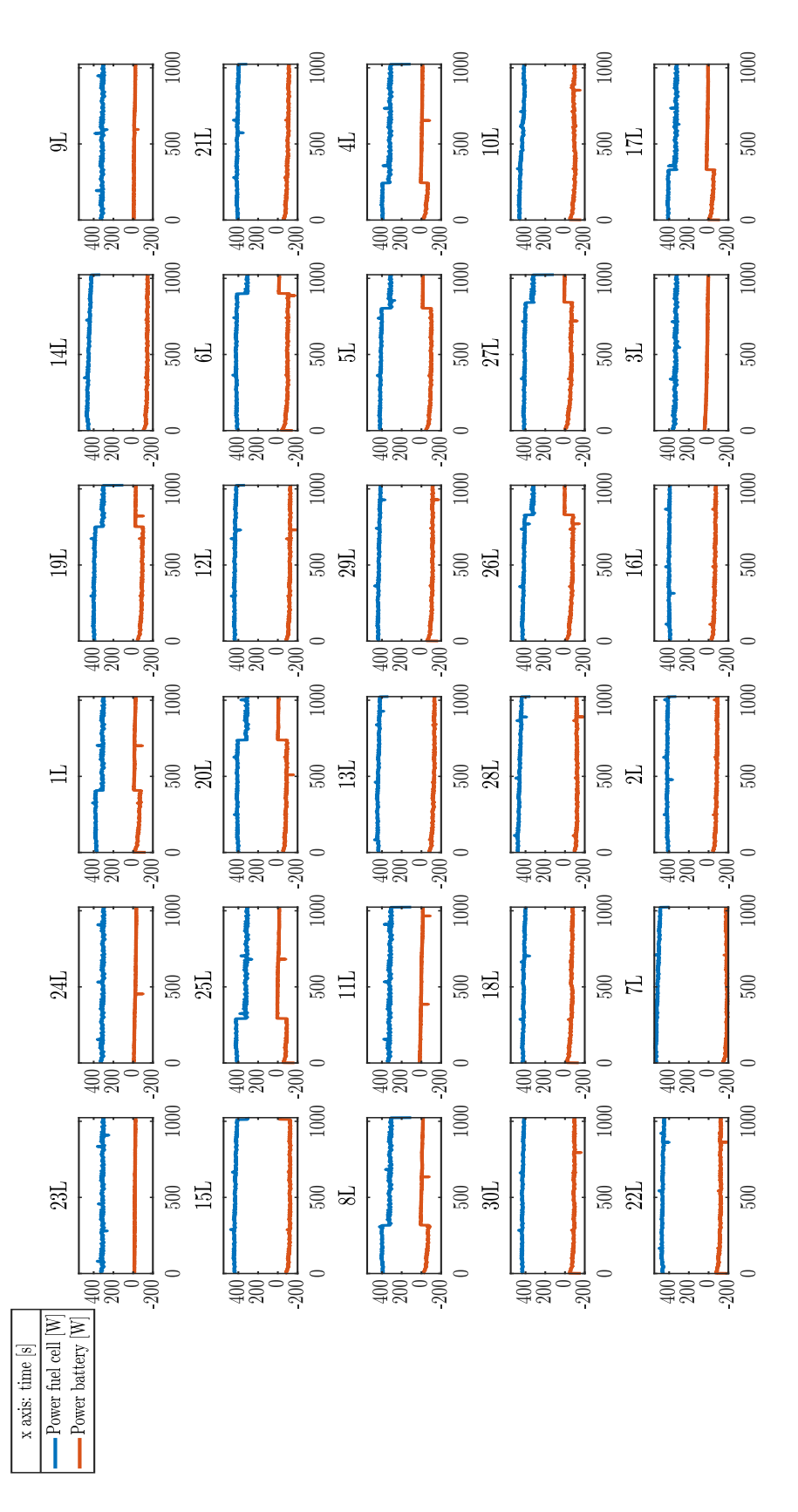


Figure D.1: Allocation of power sharing between the fuel cell and the battery for each of the V2L experiments, in the order they were performed.

Table D.1: V2L experiments per EM category

	Pbatt <0	Pbatt = 0	Pbatt <0, then Pbatt = 0
Experiments	Pbatt <0 14 15 12 21 13 29 30 28 10 22	Pbatt = 0 23 24 9 11 18 2 16 3	Pbatt <0, then Pbatt = 0 1 19 25 20 6 8 5 4 26 27
	7		17
		3	
Total	11	8	11

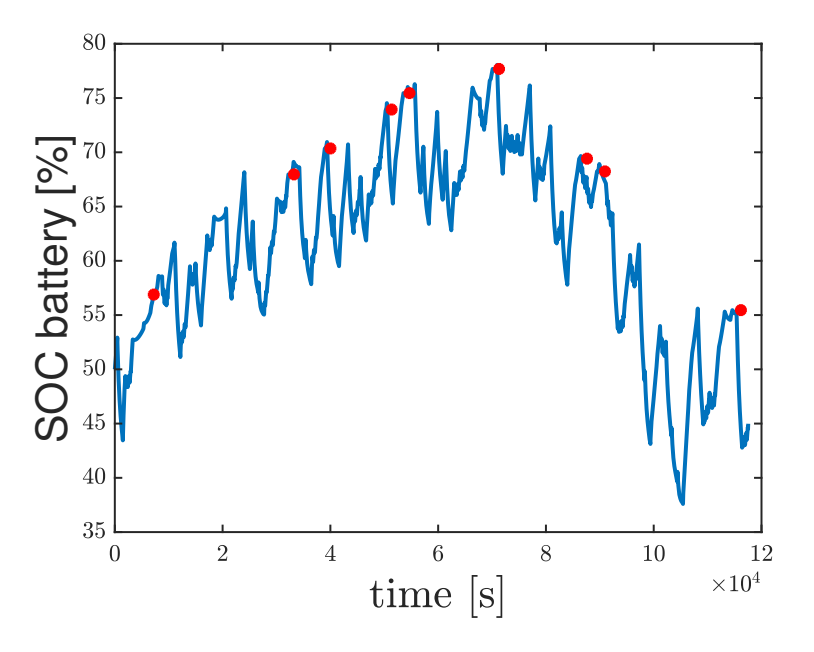


Figure D.2: SOC of the battery throughout the whole experimental period

changes in battery behavior match with a local maximum in SOC: as the battery stops charging, the SOC is not increasing anymore. However, the red dots do not correspond to the same SOC value. Occurrences of the battery that stopped charging are found for SOC varying from 57% to 78%. There is no acute SOC threshold above which the battery stops charging. Other factors than SOC might influence the charging behaviour of the battery; these have not been identified yet.

Also, the calculation of battery's SOC can be improved by taking into account the temperature in time, which has shown to have consequences on the amount of charge that can be delivered by the battery [51]. Moreover, the iterative method used here is very dependent on the initial value. Choosing 50% made the SOC values stay within 40 to 80%, which is assumed to be a reasonable operation range. It was however chosen intuitively and not based on actual measurements in the battery.



Thermal management of the PEMFC system

The efficiency of the scooter system studied was low, which means heat is being generated. Optimal fuel cell operation is comprised in a temperature window of 30-60 degrees, which implies a certain heat management system. In fact, heat is being taken up by 1. the metal hydrides, 2. a water coolant system, 3. a fan. A rough estimate of the role each of these components plays in the overall cooling is calculated here.

It is chosen to perform these calculations for an average V2G, as most heat is being produced there.

Heat generated

First, the amount of heat generated is calculated. The total amount of heat powered by the reaction of hydrogen with oxygen is:

$$Q_{\Lambda H} = HHV * n_{H2} \tag{E.1}$$

With an average hydrogen molar consumption of 0.00719 mol H2 per second, this yields 2084 W of heat. This would be the heat generated in case of combustion of hydrogen. In reality, a part of this chemical power is used as electrical power supplied to the grid. The electrical power is what is measured as Vfc*Ifc.

$$Q_{heat} = Q_{\Lambda H} - W_{elec} \tag{E.2}$$

which yields a heat rate of 1104 W.

Heat absorbed by the metal hydride

Part of this heat is being absorbed by the metal hydride, which takes up energy to liberate the hydrogen from the metal lattice. Using the van 't Hoff equation with a pressure of 10 bars, an enthalpy of -100 J/molH2 and an ambient temperature of 25degC yields an uptake rate of 24.1kJ/mol H2 liberated by the MH2. Multiplying with the average hydrogen molar consumption for V2G tests yields 173 W uptake of heat by the metal hydride. This is comparable to the results obtained in [33].

Heat absorbed by the cooling water

Water is pumped through the system for cooling. Heat taken up by the water is released to the outside via a radiator. The water system does not prevent the FCS from heating, it keeps the heating rate within a reasonable range. In order to assess the heat taken up by the water, we first estimate how much heat would be produced without the coolant water system.

$$\Delta T_{no_cool} = \frac{Q_{heat}}{MC_{syst}} \tag{E.3}$$

The heat left to be cooled is 1104-173 = 931 W. Using a MC_{syst} estimate from Lin of 2.6 kJ/K yields a warming of the system of 0.35 K/s in V2G mode and without having water pumped around. For an experiment of 1024 seconds, this would lead to a temperature increase of 366 K (or degC)!

From the experiments, we know the temperature increase throughout V2G experiments is actually 0.035 K/s, or 37 K per experiment. The water takes up the temperature difference (366-37 = 329 K). Using water's heat capacity 4.2 J/g.K and the amount of heat to be dissipated of 931 W yields a mass flow rate of water through the system of 0.7 g/s.

Heat removed by the fan

At this moment, any heat which cannot be evacuated via water cooling is blow away using a fan. When turned on, the fan can reduce the temperature at a rate of 0.05 K/s while consuming 40 W power.

System improvement

Instead of using a fan for keeping the temperature within acceptable limits, the flow rate of water can be increased.

Assumptions

In these calculations, several assumptions were made. The aerodynamic cooling effect of driving the scooter was not taken into account, as the scooter was tested still in the lab. The effect of the heat created by the BoP was not taken into account.

L. B. van Leeuwen Lottabvanleeuwen@gmail.com 4524136

